NASA Contractor Report 182197

# Microwave Characteristics of Interdigitated Photoconductors on a HEMT Structure

Scott M. Hill and Paul C. Claspy
*Case Western Reserve University*
*Cleveland, Ohio*

November 1988



Prepared for
Lewis Research Center
Under Cooperative Agreement NCC3-99

National Aeronautics and
Space Administration

# MICROWAVE CHARACTERISTICS OF INTERDIGITATED PHOTOCONDUCTORS ON A HEMT STRUCTURE


## SUMMARY

Interdigitated photoconductive detectors of various geometries have been fabricated on AlGaAs/GaAs heterostructure material. This report describes the processes used in fabrication of these devices and presents the results of a study of their optical and electrical characteristics. The fabrication process used was completely compatible with that used to fabricate MODFET's, making these detectors easily integrable for MMIC use. Detector responsivity as high as 2.5 A/W, leading to an external quantum efficiency of 3.81, was measured. It was found that response speed was independent of electrode geometry and dimensions and that all detectors had usable response at frequencies to 6 GHz, with a 3 dB frequency of 185 MHz. Because of the form of the frequency response and its independence of device geometry it is proposed that minority carrier trapping effects dominate high frequency performance. The results of DC and AC impedance measurements, as well as a small signal model of the detectors, based on those measurements is presented.

TABLE OF CONTENTS

# CHAPTER 1

# BACKGROUND

## 1.1 INTRODUCTION

In recent years there has been a great deal of work and promotion of optical fiber communication systems. The driving force being that optical fibers offer numerous advantages over other transmission media such as coaxial cable, twisted pair wire, and waveguides. These advantages include small size, light weight, flexibility, and large bandwidth. Communication systems which utilize optical fibers are often required to operate at very high data rates whether the data be analog or digital.

A communication system in its most simple form has three basic components; a transmitter, transmission medium, and a receiver. Consider the case in which the transmission medium is an optical fiber. This generates the need for high speed light sources and also high speed photodetectors if the system is to operate at high frequencies. This thesis will deal with high speed photodetectors which can be easily integrated with HEMT (High Electron Mobility Transistor) devices.

By characterizing these photodetectors it will enable MMIC (Monolithic Microwave Integrated Circuit) designers to easily incorporate the detectors in their designs. Integrated detectors

posses an advantage over discrete detectors in that there is no additional cost over that of the IC and they do not require an additional power supply. MMIC devices also occupy a much smaller area as they need not be packaged separately. There are also fewer possibilities of losses due to couplers and overall system performance should increase.

## 1.2 ADVANTAGES OF FIBER OPTIC LINKS

Why use fiber optic links at all, why not use coax or even free space transmission? In free space you do not pay for the medium and it only attenuates as $1/r^2$. In guided systems such as coax, waveguides and optical fiber the signal attenuates exponentially and is definitely not free.

For long signal paths it would seem that free space transmission is the way to go. Free space transmission, however, is impractical except for satellite communications. This is because most communication systems are on earth where the signal suffers from atmospheric attenuation and distortion. In addition if very high frequencies are to be used then the transmission is basically limited to line of sight. This imposes an approximate transmission length of 20 Km which is susceptible to disturbances ranging from an electrical storm to a flock of birds.

It would appear that free space transmission is out for most situations. Why use fiber optic links and not coaxial cable? Optical fibers offer several advantages over coax such as low attenuation, low cost, low weight, immunity from electrical interference and high bandwidth [1]. Fiber optic links are often

operated at wavelength of 1.3 microns. This is because the silica fibers exhibit their lowest loss of about 0.47 dB/Km at this wavelength [2].

Operation at this wavelength, however, requires the use of ternary or quaternary compound semiconductor sources which are both more expensive and less developed than sources in the 800 nm range. Silica fibers exhibit attenuations of approximately 2 dB/Km at this wavelength [3]. In contrast, RG-400 coaxial cable exhibits 1115 dB/Km attenuation [2] when operated at 5 GHz. Waveguides can exhibit attenuation rates as low as 0.6 dB/Km but are very expensive due to the large amount of metal needed for transmission over long distances [4].

One application in which almost all of the advantages of fiber optic links could be used is in signal distribution in a phased-array antenna. The number of elements in these antennae is constantly increasing. Soon conventional methods, hollow metal waveguides, will limit the number of elements, however, the small size and flexibility of fiber optic links may provide the solution [5,6]. By implementing systems utilizing MMIC transmitter and receiving units to control amplitude and phase with optical feeds the number of elements and frequency range should increase significantly. Crosstalk between the closely spaced elements should also be nearly eliminated. In addition, the much lower weight of the optical fibers makes them ideal for use in satellites where weight is a critical factor due to limited launch payloads.

## 1.3 WHY A HEMT STRUCTURE?

The HEMT or MODFET (Modulation-Doped Field-Effect Transistor) is quickly demonstrating its superiority over other technologies (silicon, germanium arsenide, etc.) for high speed applications. It switches on or off in as little as 12.2 ps for digital applications. It can also serve as an analog amplifier at frequencies up to 70 GHz and is soon expected to exceed 100 GHz [7].

The HEMT also posses several advantages other than speed, over devices such as vertical FETs, bipolar junction transistors, CMOS, etc. The vertical FET, for example, has demanding lithography requirements and Josephson Junction devices are difficult to fabricate. The HEMT has a definite advantage over MESFET's at room temperature with higher mobility of 8000 $cm^2/Vs$ vs. 4000 $cm^2/Vs$. This mobility increases dramatically when cooled to 77°K (135,000 $cm^2/Vs$) [8]. Similarly, the HEMT possesses an advantage in higher transconductance - 400 millisiemens per millimeter of gate width at 77°K and 270 mS/mm at 300°K versus 230 mS/mm for the MESFET and 80 mS/mm for the MOSFET [9]. The power dissipations are in the ratio of 1:2.6:25, once again demonstrating the superiority of the HEMT.

Since the HEMT is clearly superior for amplifier applications it becomes desirable to fabricate and characterize photodetectors which may be easily integrated with the MODFET's. If such detectors can indeed be fabricated they may then be used in integrated photoreceivers.

## 1.4 PREVIOUS WORK

In 1977 Baack et. al. [10] drew attention to the use of a GaAs MESFET as a high speed optical detector. Since that time there has been considerable effort in developing and characterizing high speed detectors which are easily integrated into MMIC usage. It has been shown that the gain and $I_{d_{ss}}$ of a GaAs MESFET may be controlled by a modulated light source in the same manner as when varying the $V_{g_s}$ [25]. By far the greatest amount of work has been done in the area of GaAs MESFET's but in recent years, with the emergence of the MODFET, there has been increasing effort in developing detectors on heterostructure materials.

The GaAs MESFET has probably received the most attention as a potential high-speed photodetector. There have been numerous papers [11-16] on the characteristics and mechanisms of this photodetection process. The GaAs MESFET, however, suffers from poor coupling efficiency due to the small electrode spacing (0.5 - 1.0 μm) and surface reflection. These devices, however, may exhibit gain and very high responsivity. Gains on the order of 5-10 have been reported [11] and responsivities as high as 1300 A/W [13]. The gain of the detectors typically begins to roll off in the MHz range but usable gain still exists out beyond 1 GHz. Rise times of 46 ps with Full Width at Half Maximum (FWHM) pulse widths of 73 ps have also been reported [16] but suffer from a long optical tail. It has been proposed that by changing the geometry of the FET's it may be possible to extend the frequency response out to 10 GHz.

As an alternative to the FET structure straight gap and interdigitated detectors have been fabricated on GaAs [17-19]. Improved alignment and coupling efficiencies allow these devices to show improved gain over that of the MESFET's [19], however, they still suffer from a relatively low bandwidth. The response still typically rolls off well before the GHz range. The high gain compensates for this, though, leading to higher gain-bandwidth products.

Perhaps the fastest detectors yet reported are those which utilize Schottky contacts. The geometries of these detectors vary from circular [20,21] to gap [22,23] to interdigitated [24]. These Schottky barrier photodiodes typically exhibit a flat frequency response up to about 20 GHz although a 3 dB bandwidth of 100 GHz has been reported [23]. These detectors typically suffer from a low quantum efficiency with the average being about 25%.

For longer wavelength applications (1.0-1.6 μm) detectors on an $Al_xIn_{1-x}As/Ga_yIn_{1-y}As$ heterostructure have been developed. This structure nominally consists of an InP semi-insulating substrate on which the following layers are grown: an undoped $Ga_yIn_{1-y}As$ layer, a spacer of undoped $Al_xIn_{1-x}As$, an n doped layer of $Al_xIn_{1-x}As$, and an optional layer of n doped $Ga_yIn_{1-y}As$. The electrode geometries range from interdigitated electrodes [26-28] to straight gap conductors [29,30] to that of a FET [31]. The reported pulse response of these detectors show a typical rise time of 80 ps and a FWHM width of 200 - 600 ps.

These detectors also exhibit the long decaying tail which is on the order of 1 - 3 ns long. Some complete integrated photoreceivers have been built and exhibit a 2-Gbit/s receiver sensitivity with a bit error rate less than $10^{-9}$ [28].

Of greater interest in this thesis are the detectors fabricated on the $Al_xGa_{1-x}As/GaAs$ heterostructure. These detectors are designed for use with shorter wavelengths (0.6 - 0.84 μm). The most common structure is that of the FET [32-35] although interdigitated structures have also been investigated [36]. The analysis of these detectors has been largely carried out in the time domain with the frequency response being inferred from the pulse response.

The pulse response of the MODFET's showed a fast rise time (12 ps) and a FWHM pulse width of between 20 ps and 27 ps [32-34]. The external quantum efficiency of these detectors has been measured to range from slightly over 60% to as high as 630% [33]. The interdigitated photoconductor also exhibited a high gain and fast rise time. While the prevalent optical tail is present in the interdigitated detector there is no mention of its existence made in connection with the MODFET's.

Some effort has been made to improve detector performance by using unique geometries and mounting techniques. Chen et. al. [36] have fabricated a gap detector with a back gate electrode. This back gate is biased so as to "sink" the minority hole carriers which lead to the long optical tail. The fall time of the detector's response time is reported to drop from 1 ns down to 80

ps with little adverse affect on the responsivity, leading to nearly an order of magnitude increase in gain-bandwidth product. Another detector has been reported which is apparently able to operate free of any dc bias [37]. This detector, however, suffers from a very low sensitivity (0.04 A/W). Other unique structures have also been proposed to increase the responsivity and gain of detectors [38,39].

## 1.5 SYNOPSIS OF WORK

The fabrication of the detectors will be discussed in Chapter 2. This will include a detailed description of each step in the fabrication process. Also included in Chapter 2 are the methods used for mounting and bonding the detectors for test purposes.

The frequency response and responsivity of the detectors will be presented in Chapter 3. The effect of different electrode geometries will be discussed along with the response mechanism. Quantum efficiency values will be derived from the responsivity measurements.

Both DC and AC impedance measurements will be examined in Chapter 4. The effects of varying bias and incident light power will be examined in both a qualitative and quantitative manner. A corresponding small signal model for the detectors will be inferred from the measurements.

# CHAPTER 2

# FABRICATION AND MOUNTING OF PHOTODETECTORS

## 2.1 INTRODUCTION

This chapter discusses the fabrication and mounting of the detectors reported in this thesis. A review of the inherent properties of the heterostructure is also given. Each fabrication step is presented in a detailed recipe format which should allow easy duplication. The two different schemes used for mounting the detectors are also presented along with the motivation for each.

## 2.2 PHOTODETECTOR MATERIAL

The photoconductors reported in this thesis were fabricated on the HEMT structure shown in Fig. 2.1. The heterostructure, supplied by the Perkin-Elmer Corporation, was grown by Molecular Beam Epitaxy (MBE) on a semi-insulating GaAs substrate. The layers grown were; a 1 μm layer of undoped GaAs, a 20 Å spacer of undoped $Al_{0.3}Ga_{0.7}As$, 300 Å of $n^+$ $Al_{0.3}Ga_{0.7}As$ ($n = 2x10^{18}$ $cm^{-3}$), and finally a 400 Å capping layer of $n^+$ GaAs ($n = 2 \times 10^{18}$ $cm^{-3}$). The capping layer is provided to help in the formation of Ohmic contacts and to prevent oxidation of the AlGaAs prior to processing.

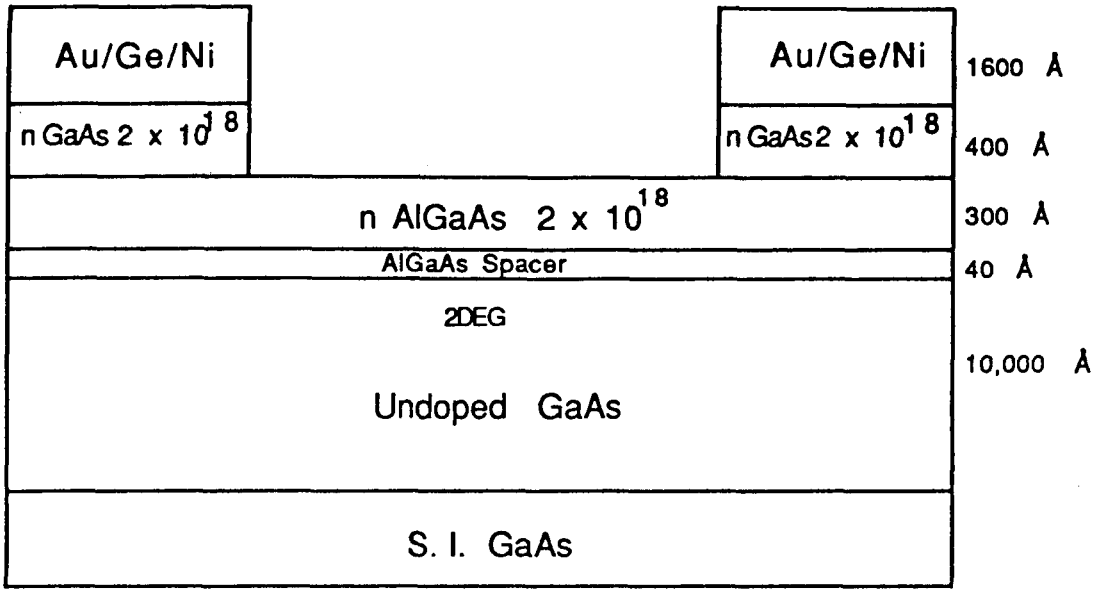


Fig. 2.1. HEMT structure.

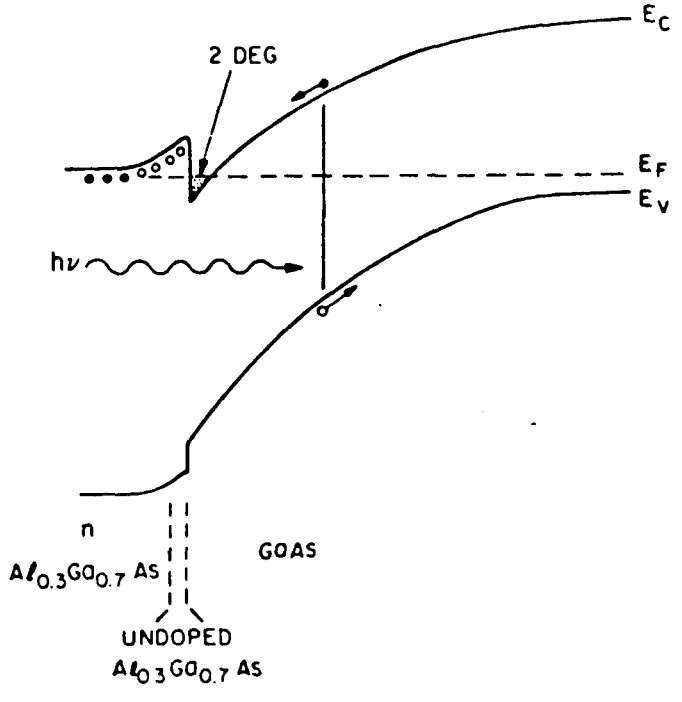


Fig. 2.2. Energy band diagram.

Due to its high band-gap energy the AlGaAs window is essentially transparent to the incident radiation (820 nm). This means that almost all of the photon absorption and, therefore, electron-hole pair generation is occurring within the undoped GaAs layer.

The HEMT takes advantage of the fact that electrons have a higher mobility in undoped GaAs than in doped GaAs. The HEMT is a heterostructure, it consists of two different materials GaAs and AlGaAs in the same continuous crystalline structure, as opposed to the MESFET, previously the fastest transistor, which consists of a uniform material with different dopant levels.

The GaAs MESFET is doped in order to generate carriers. The electrons created in this generation process, however, must share space with the donors and the ensuing electron-scattering by the donors reduces the electron mobilities. The electrons in the HEMT material diffuse toward the lower band-gap material, GaAs, and are confined by the energy barrier at the heterojunction while the holes are forced away from the heterojunction by the band bending (see Fig. 2.2). This yields the so called two dimensional electron gas (2DEG) which results in very large electron velocities for low values of bias voltage [7-9,40-41].

## 2.3 DETECTOR GEOMETRIES

Interdigitated electrode geometries are used because they increase the effective active area while keeping the transit distance small and are simple to fabricate. The fabrication process is compatible with that of MODFET's and will be described in detail in the following sections. Interdigitated electrodes also posses advantages over conventional straight gap photoconductors. If the gap length of the straight gap detector is equal to the interelectrode spacing of the interdigitated detector and the finger length is equal to the gap width then the interdigitated detector will exhibit a responsivity N times greater than the straight gap, where N is the number of electrodes [42]. While the interdigitated detector will have a slightly higher intrinsic capacitance it is not enough to significantly reduce frequency response. Because they are attractive as photoconductors there's been a good deal of work with interdigitated geometries on a variety of structures.

The detectors reported in this thesis have three different contact shapes and five combinations of electrode width and gap spacing. The contact pads are either "bow-tie", "dumb-bell", or rectangular in shape (see Fig. 2.3). The rectangular detectors are totally isolated on the mesa, whereas the "bow-tie" and "dumb-bell" detectors have only the finger region on the mesa. The remainder of the contact pad flows over the edge of the mesa onto the undoped GaAs.

The interdigitated fingers have five different combinations

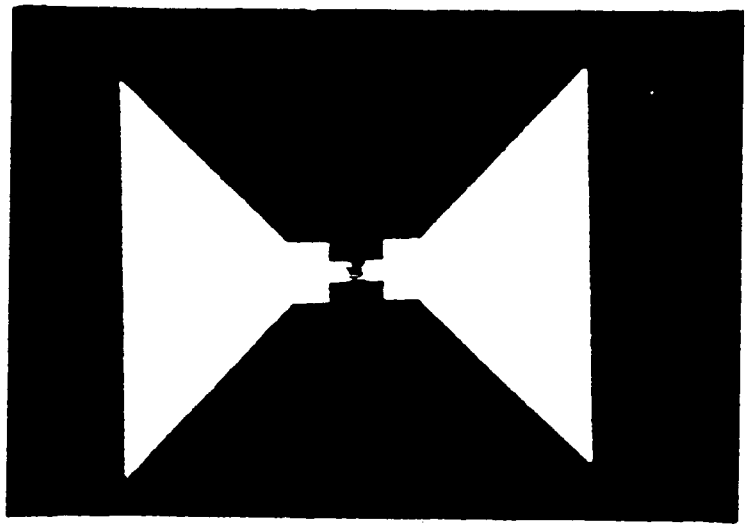

a) "Bow tie" geometry.

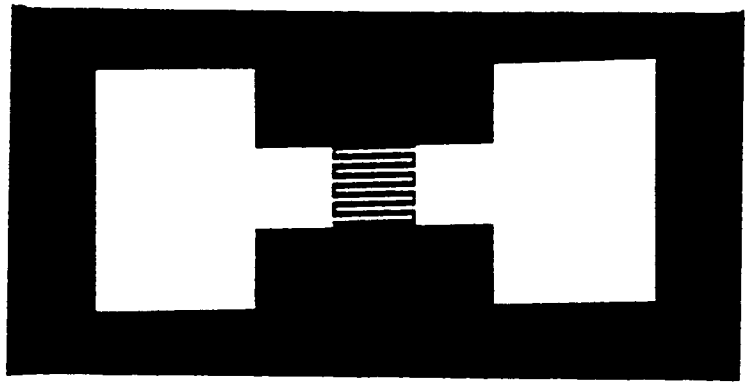

b) "Dumbbell" geometry.

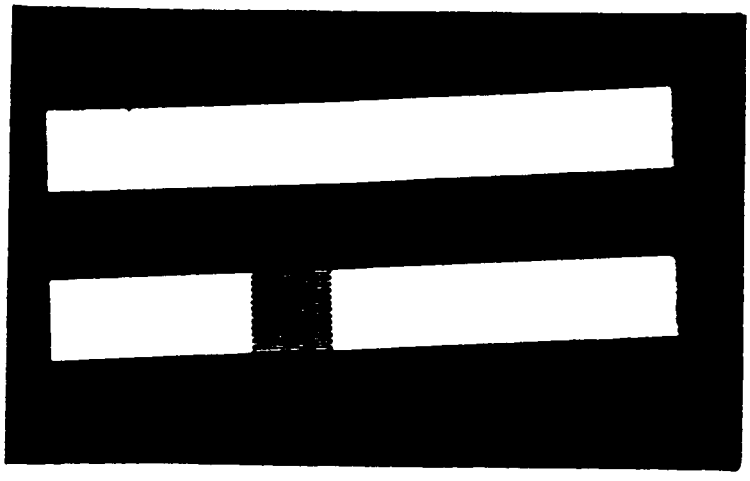

c) Rectangular geometry.

Fig. 2.3. Detector contact pads.

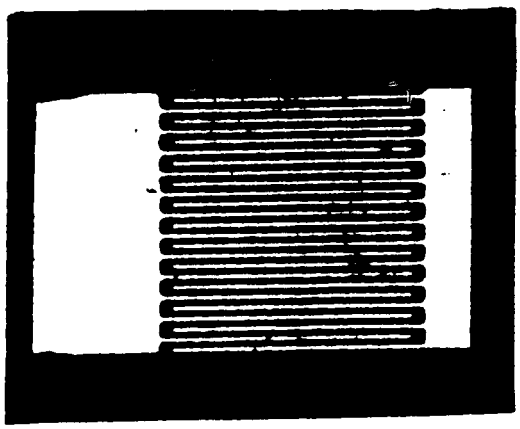

a) 1 x 1 µm

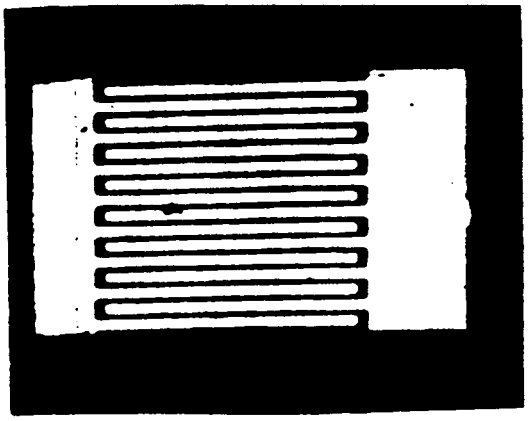

b) 2 x 1 µm

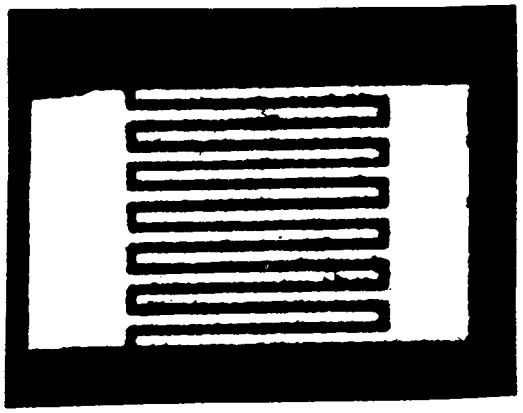

c) 2 x 2 µm (13 fingers)

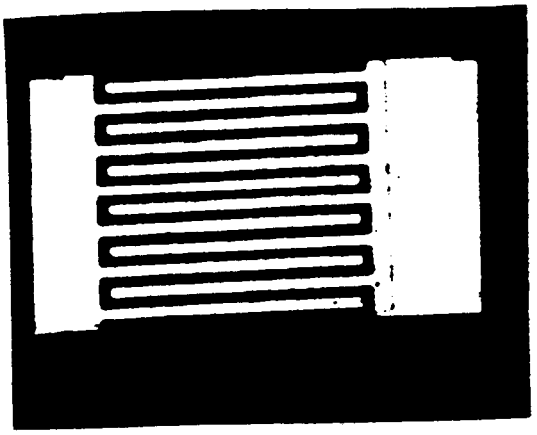

d) 2 x 2 µm (12 fingers)

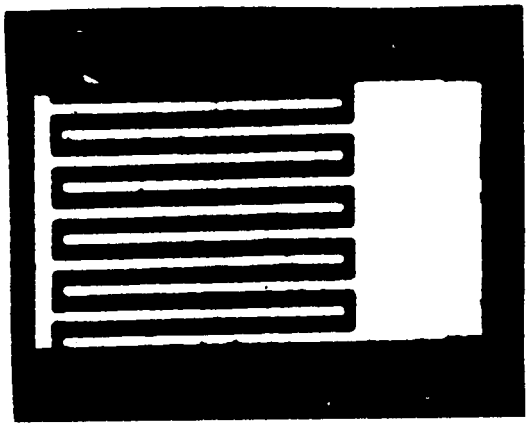

e) 2 x 3 µm

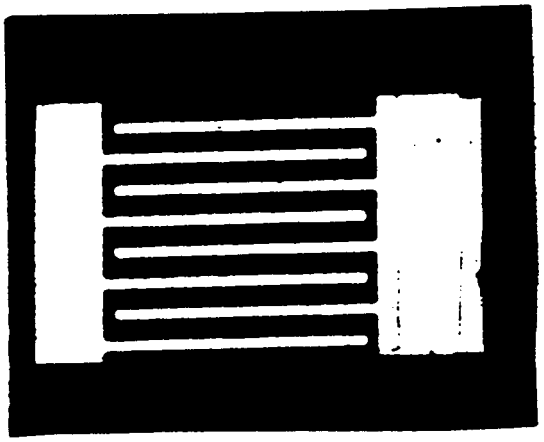

f) 2 x 4 µm

Fig. 2.4. Interelectrode geometries.

of electrode width by gap spacing. The combinations are; 1 x 1 μm, 2 x 1 μm, 2 x 2 μm, 2 x 3 μm, and 2 x 4 μm. In all cases the total active area is 50 x 50 μm. Photographs of the various geometries may be seen in Fig. 2.4. The advantage gained between the 2 x 1 μm and 1 x 1 μm detectors is that for the 1 x 1 μm detectors only 50% of the active area is covered by the metal fingers whereas, 67% of the 2 x 1 μm detector's active area is covered by the fingers.

## 2.4 THE PHOTOLITHOGRAPHIC PROCESS

The photodetectors reported in this thesis were fabricated on the structure described in section 2.2. The detectors were fabricated using well known photolithography techniques [43] at the NASA Lewis Research Center. During the fabrication process several steps were carefully characterized and will be described in detail in the appropriate sections. The basic steps in the photolithography process are 1) cleaning of the sample, 2) mesa isolation, 3) placement of ohmic contact patterns, 4) ohmic contact evaporation, 5) removal of capping layer, 6) alloying of ohmic contacts, 7) cleaving sample into separate detectors. All of the preceding steps were first performed on semi-insulating GaAs to insure that there were no problems and then on the HEMT material of the actual detectors.

## 2.5 CLEANING OF WAFER

It is necessary to ensure that the wafer be cleaned of all dirt or any substance which may effect the lithography process. All chemicals used in the fabrication process are of electronics

grade. The sample is first cleaned using an acetone bath in the ultrasonic cleaner for five minutes and then rinsed using clean acetone. After the acetone rinse the sample is once again placed in the ultrasonic cleaner, but this time in methanol. The sample is then rinsed in deionized (D.I.) water for two minutes to remove any residual methanol. A weak etch is then performed to remove any oxides which may have been formed on the surface. The etch used is a 1:1 $HCl:H_2O$ solution for thirty seconds. A final rinse in the D.I. bubbler is then followed by blow drying the sample with clean $N_2$.

## 2.6 MESA ISOLATION

Mesa isolation is necessary to ensure the electrical separation of the individual detectors. Mesa isolation consists of masking off each area where a detector is to be placed and etching the rest of the sample down into the undoped GaAs. The first step is to bake the sample at 110°C for 30 minutes to prepare it for the application of photoresist. Once the sample has cooled to room temperature photoresist AZ4110 is spun on at 4000 rpm. This produces a layer of photoresist approximately 1.1 μm thick (see Fig. 2.5a). The sample is further baked at 90°C for 20 minutes to harden the photoresist. The sample is cooled for at least 30 minutes to allow for humidity absorption.

The sample must now be exposed in order to provide the proper mesa pattern. Care should be taken when transporting the sample that it is not exposed to ultra-violet light (i.e. filtered lights should be used in the processing lab). Place the

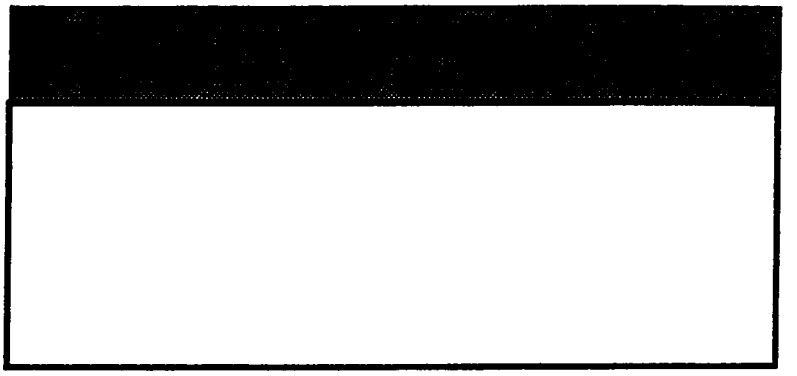

a. Wafer with 1.1 μm photoresist layer.

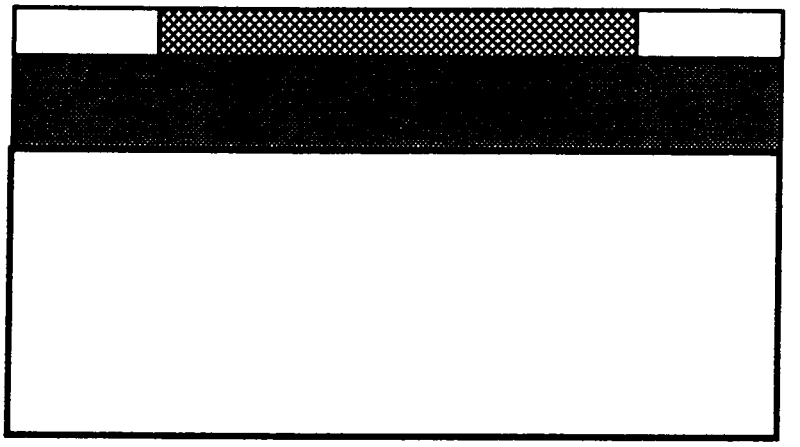

b. Alignment of mask and exposure of photoresist.

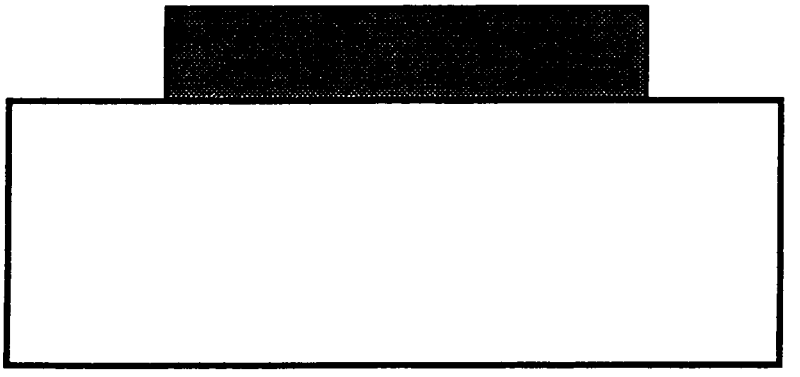

c. Development of photoresist.

Fig. 2.5. Steps in photolithography process.

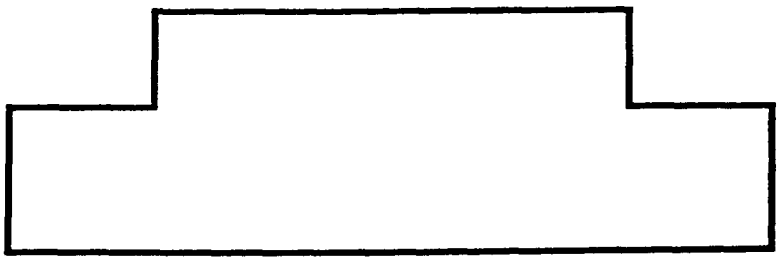

d. Mesa formation.

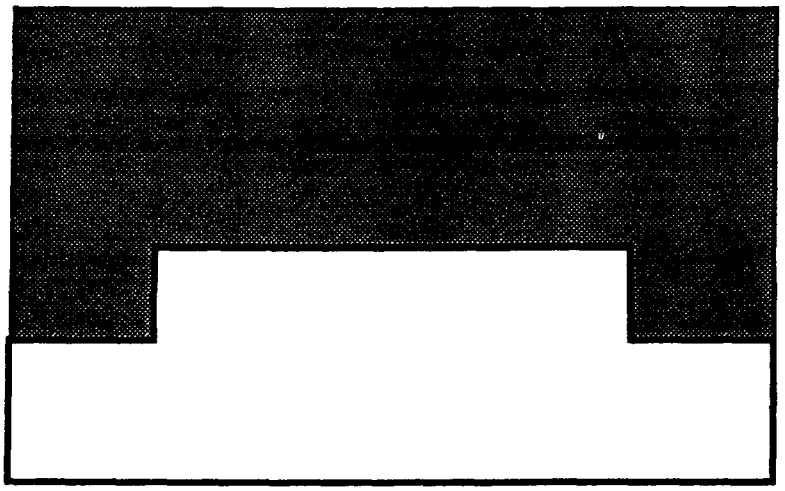

e. Wafer with 4000 Å photoresist layer.

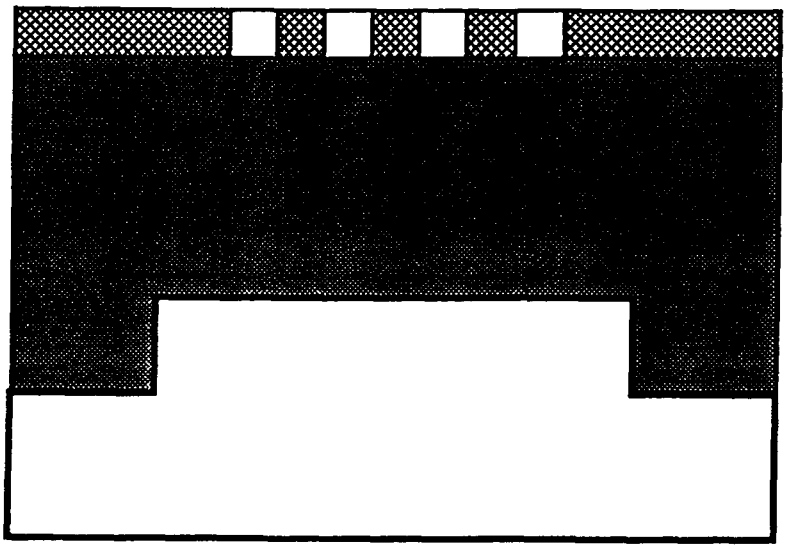

f. Alignment of contact mask and exposure of photoresist.

Fig. 2.5. (cont.)

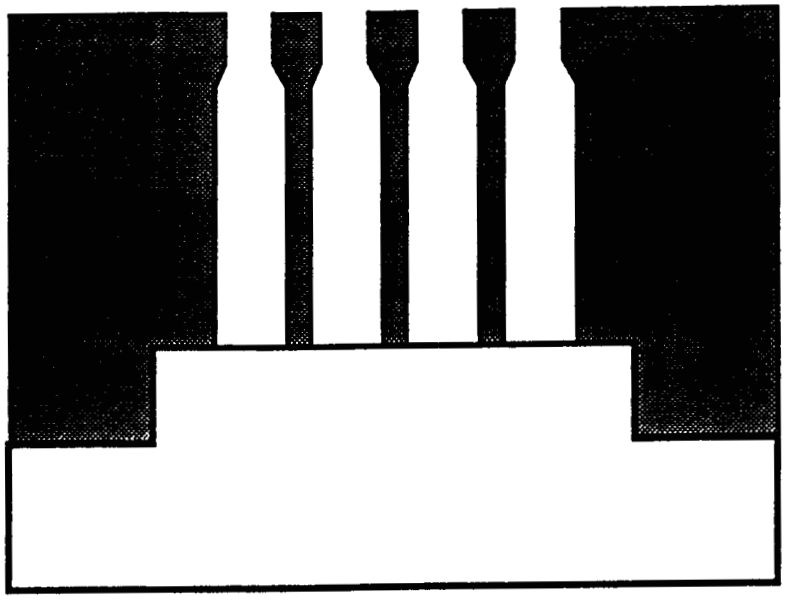

g. Development of photoresist with clorobenzene soak.

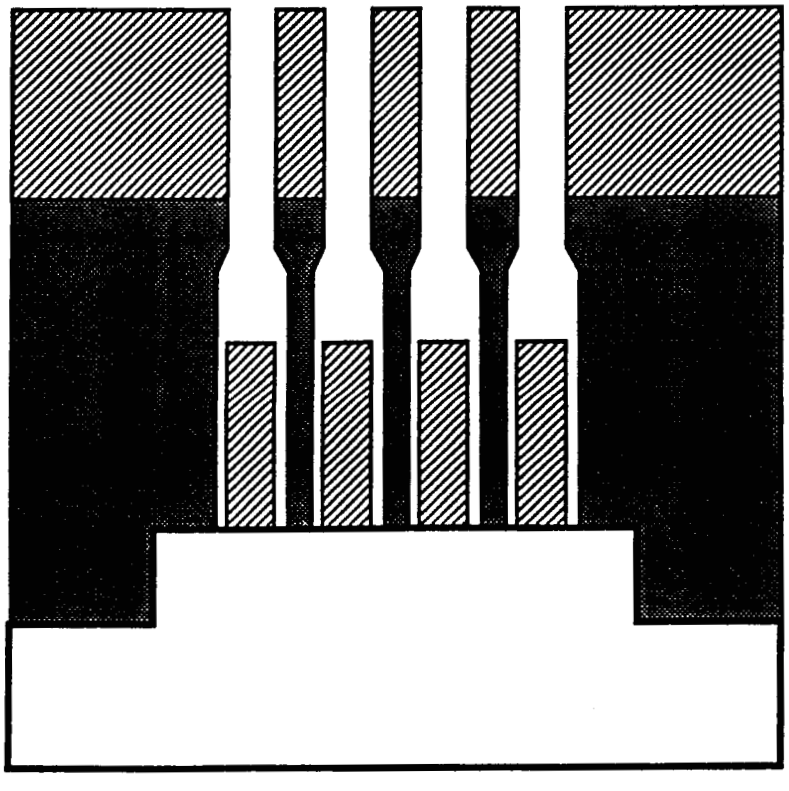

h. Evaporation of ohmic contacts.

Fig. 2.5. (cont.)

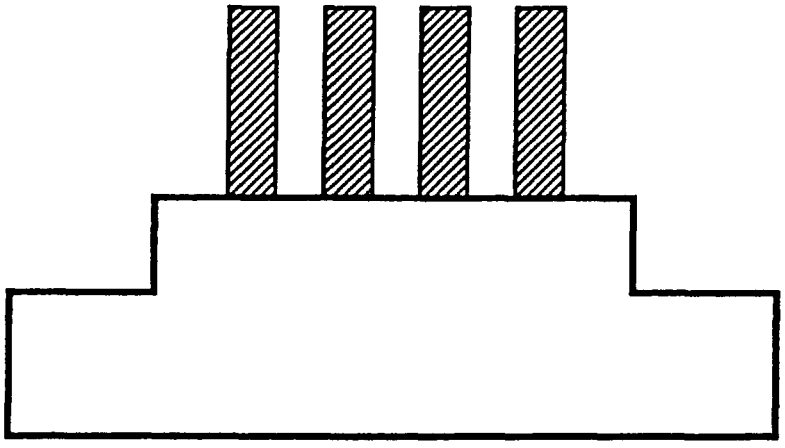

i. Lift-off of photoresist.

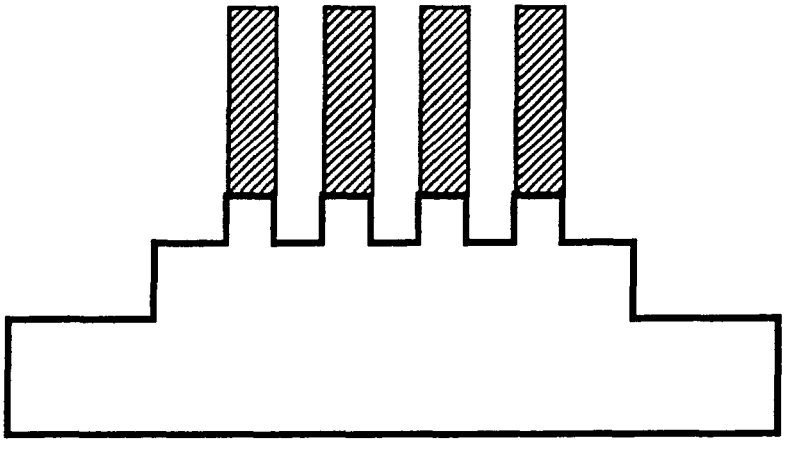

j. Cap layer etch.

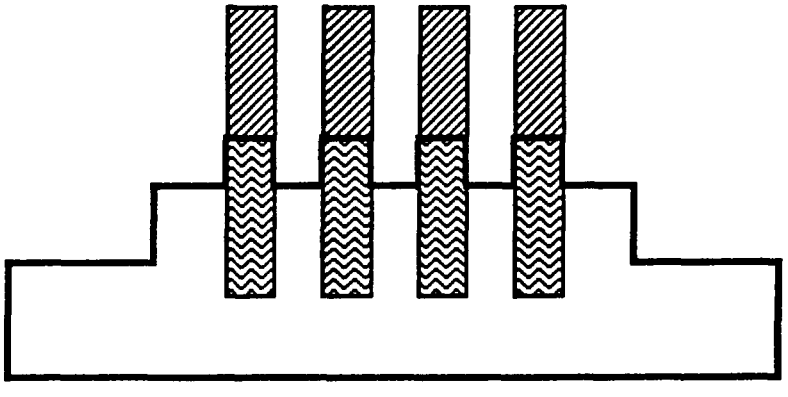

k. Alloying of ohmic contacts.

Fig. 2.5. (conclusion)

sample in the mask aligner and align the mesa mask over the sample (see Fig. 2.5b). Expose the sample for 30 seconds at 20 $mW/cm^2$. The sample is now developed in 4:1 developer. Develop for 1 minute 30 seconds in 4:1 developer and rinse for 2 minutes in D.I. water bubbler.

Now that the mesa pattern has been deposited on the sample (see Fig. 2.5c) it is necessary to etch down to the undoped GaAs. The etchant used is a 3:1:0.75 solution of phosphoric acid ($H_3PO_4$): hydrogen peroxide ($H_2O_2$): water ($H_2O$). The etchant is cooled in an ice bath to approximately 0-3°C in order to reduce the etch rate and give more precise depth control. The etch rate at 3°C is approximately 220 angstroms per minute and it is etched for 5 minutes to produce a 0.11 m mesa (see Fig. 2.5d). The sample is rinsed in D.I. water to halt the etch and then blown dry with $N_2$.

## 2.7 CONTACT PATTERN DEPOSITION

Now that the mesas have been formed it is possible to create the ohmic contact patterns. This process begins the same as the mesa creation by baking for 30 minutes at 110°C. Photoresist AZ4040 is then spun on at 4000 rpm. Photoresist AZ4040 is used instead of AZ4110 due to problems encountered in the initial fabrication of the detectors. The 1 x 1 μm detectors exhibited partial or total loss of detail in the finger region. It was theorized that the small finger width and gap spacing was in essence acting as a diffraction grating. This problem could be solved in one of two ways, by using a shorter wavelength to ex-

*pose* the resist or by using a thinner resist. The later option was chosen. AZ4040 yields a layer of photoresist approximately 4000 angstroms thick (see Fig. 2.5e).

The sample is again put in a soft bake at 90°C for 20 minutes and then allowed to cool for 30 minutes. The ohmic contact mask is aligned over the mesas and the sample exposed for 15 seconds (see Fig. 2.5f). The shorter exposure time is to compensate for the thinner resist. After being exposed the sample is not immediately developed. It is first put in a clorobenzene soak for 5 minutes. It is rinsed and blown dry after the soak. The clorobenzene soak is used to create a "lip" to aid in lift-off. The clorobenzene causes the top layer of the photoresist to become harder, thereby slowing the development rate through that layer. It develops the lower portion faster causing the creation of a lip (see Fig. 2.5g).

The sample is developed in 4:1 developer to reveal the ohmic contact pattern. The development time is nominally 90 seconds but may vary. Care must be taken to not overdevelop while at the same time making sure that all of the photoresist is removed. After each period in the developer the sample is rinsed in D.I. water to stop the developing.

## 2.8 EVAPORATION AND ALLOYING OF OHMIC CONTACTS

An important factor in the performance of the photodetectors is the existence of good Ohmic contacts. The contacts must reach down to the 2DEG for optimum performance. The metallization used for the contacts was 300A AuGe/ 100A Ni/ 1600A Au followed by a

90 second 700°C alloy cycle. This metallization and alloy cycle were developed at Cornell University.

The metals used for the contacts were evaporated onto the detector samples sequentially at a rate of 1 Å/sec. (see Fig. 2.5i). Following evaporation of the metals it is necessary to "lift-off" the metal from the areas covered with photoresist. A 10 minute acetone soak is usually sufficient to this. The acetone dissolves the photoresist and the metal above the photoresist then "lifts-off" the sample. If lift-off does not occur a gentle agitation may be used to initiate the process. Care must be taken when choosing a metallization that the total thickness of metal does not exceed the difference between the photoresist thickness and mesa height. If the difference is exceeded then it will be impossible to achieve lift-off because the acetone will be unable to attack the photoresist.

Following lift-off it is necessary to alloy the metallization. This is accomplished by placing the sample on an open-faced quartz boat in a furnace at 700°C for 90 seconds with flowing $N_2$. This will allow the AuGe to diffuse down to the undoped GaAs and create Ohmic contacts. Insertion into and removal from the furnace are performed quickly, (2-3 seconds).

## 2.9 REMOVAL OF CAPPING LAYER

Also important to detector performance is the removal of the $n^+$ GaAs capping layer. This layer has a very high doping concentration ($2 \times 10^{18}$ $cm^{-3}$) and the dark current contribution due to it totally swamps the photoconductive effect if not removed.

Once the capping layer is removed it is possible to observe the photoconductive effect in the detectors. Fig. 2.6 qualitatively demonstrates how removal of the capping layer effects the DC response of the detectors to light from a microscope objective. As can be seen in the figure, when an etch depth of only 350 Å is achieved the current is very large and shows no dependence on the incident light level. When the etch depth reached 400 Å the magnitude of the current dropped by a factor of 4 but exhibited a large dependence on the incident light level. An etch depth of 460 Å shows this same dependence on light but at a decreased current level.

The ideal etchant to use would be one which etches only GaAs and not AlGaAs. To this end some research was done in this area. A superoxyl etch of 30% $H_2O_2$ has been reported to have a selectivity of ten [44]. The etch rate for the superoxyl etchant is highly dependent on PH level. It was reported to be 1000 Å/min. at a PH of 7.04. These results, however, were unable to be reproduced at the Lewis Research Center. There was not a linear relationship between etch time and etch depth, nor was there a well-defined non-linear relationship. In fact, it proved impossible to repeat any time versus depth measurements. Therefore, the same etch that was used for mesa isolation was also used to remove the capping layer. The etch rate in $n^+$ GaAs is 200 Å/min. as opposed to the 220 Å/min. in the composite material. This is due to the fact that the etch rate in AlGaAs is greater than in

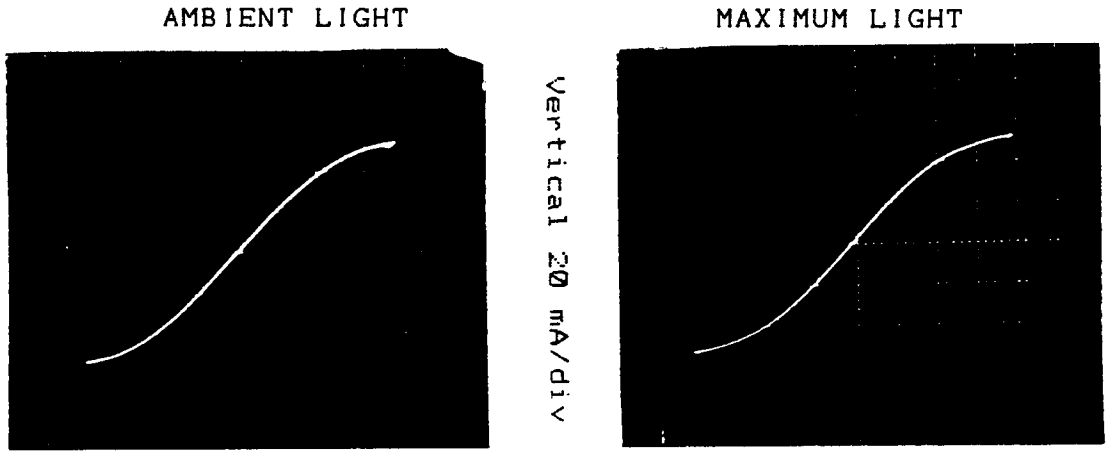


a. 350 Å removed. (Ordinate = 20 mA/div)

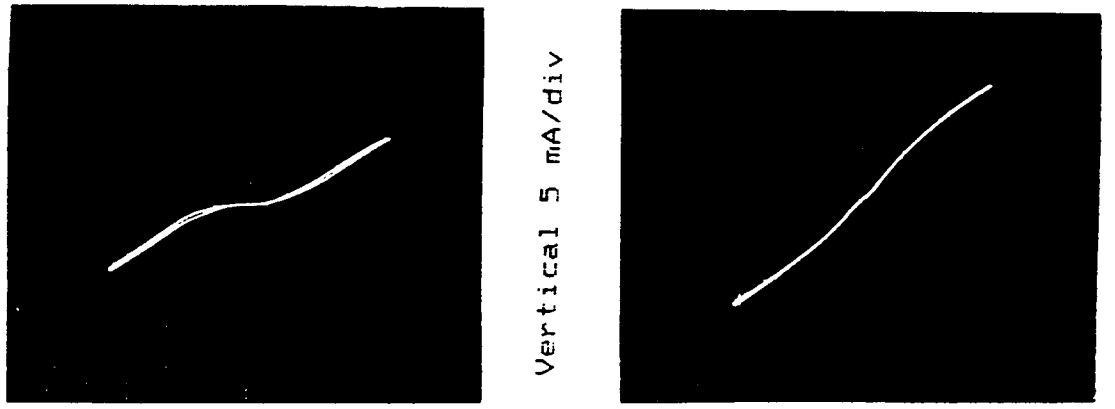


b. 400 Å removed. (Ordinate = 5 mA/div)

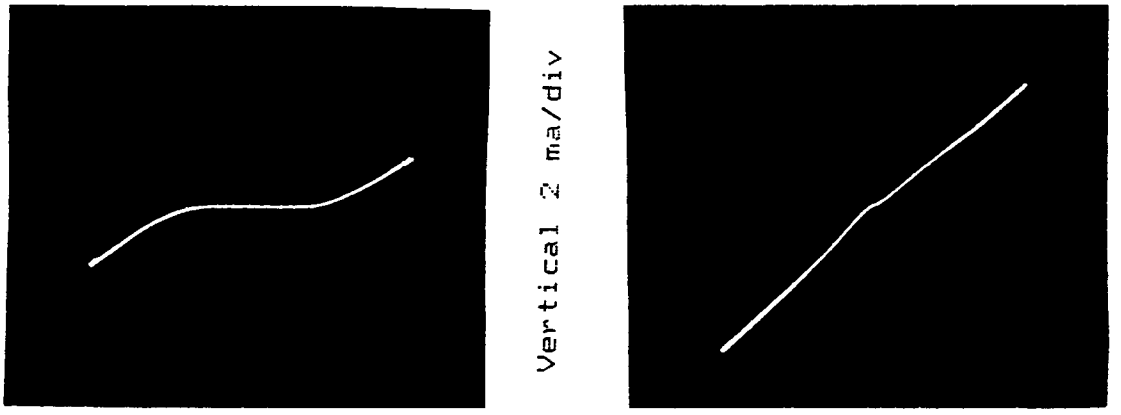


c. 460 Å removed. (Ordinate = 2 mA/div)

Fig. 2.6. Effect of cap layer removal on I-V characteristic. (Abcissa = 0.5 V/div in all cases).

**GaAs.** Accordingly, the samples were etched for 120 seconds to produce the desired 400 Å etch (see Fig. 2.5j).

## 2.10 CLEAVING OF SAMPLE

After the detectors were fabricated it was necessary to separate the individual detector types so that they may be mounted. The process whereby the sample is cleaved is very simple. Lines are scribed on the surface of the sample where breaks are desired by using a diamond tipped scribe. Once all the scribe marks have been made the sample is hermetically sealed in a sterile plastic bag. This is to prevent any dust from becoming embedded in the detectors when they are cleaved. The sample is cleaved by placing the sealed sample on a slightly curved piece of plexiglas and gently pressing down with a cylinder on the scribe lines.

## 2.11 MOUNTING OF PHOTOCONDUCTORS

The interdigitated photoconductors were mounted in one of two ways. Initially the photoconductors were mounted on aluminum blocks which served has both a pedestal and ground plane. The Aluminum blocks measured approximately 125 mm x 125 mm x 190 mm and were polished on all sides but the bottom to allow for proper bonding adhesion and contact with SMA connectors. In addition a hole was drilled and tapped to allow for the easy attachment and removal of SMA connectors. A ceramic piece with a 50 Ohm gold microstrip transmission line was then mounted on the top face with a non-conducting epoxy. The ceramic piece measured approximately 95 mm x 32 mm. The detector was then mounted on the

ceramic piece with the non-conducting epoxy.

Bonding between the detectors and the microstrip line and ground plane was accomplished by using 1 mil gold wire and a wedge bonder. One gold wire was attached to the right contact pad and microstrip transmission line, the other to the left contact pad and Aluminum ground plane (see Fig. 2.7). The bond to the ground plane was made using silver-epoxy. This was done due to adhesion problems between the gold wire and aluminum. Finally a SMA end-launcher of the type used for microstrip transmission line to coaxial was aligned over the microstrip transmission line and attached using a small screw.

Due to concern over possible contact problems between the end-launcher and microstrip line as well as possible capacitive effects a second mounting scheme was developed. A semi-rigid piece of 50 Ohm coaxial cable approximately 400 mm long had an SMA connector attached to one end. The other end was ground at a 45 degree angle to produce a plane for mounting the photodetectors. The detectors were mounted on the teflon between the center conductor and exterior shield using the non-conductive epoxy. The same gold wire and bonder used in the prior method were also utilized for this method. One gold wire was bonded to the left side of the detector and center conductor. Another connects the right side and ground shield (see Fig. 2.8). This scheme allows for shorter lengths of wire ( $< 2mm$ ) and eliminates the need for any silver-epoxy in that bonding to the copper may be directly accomplished with the wedge bonder.

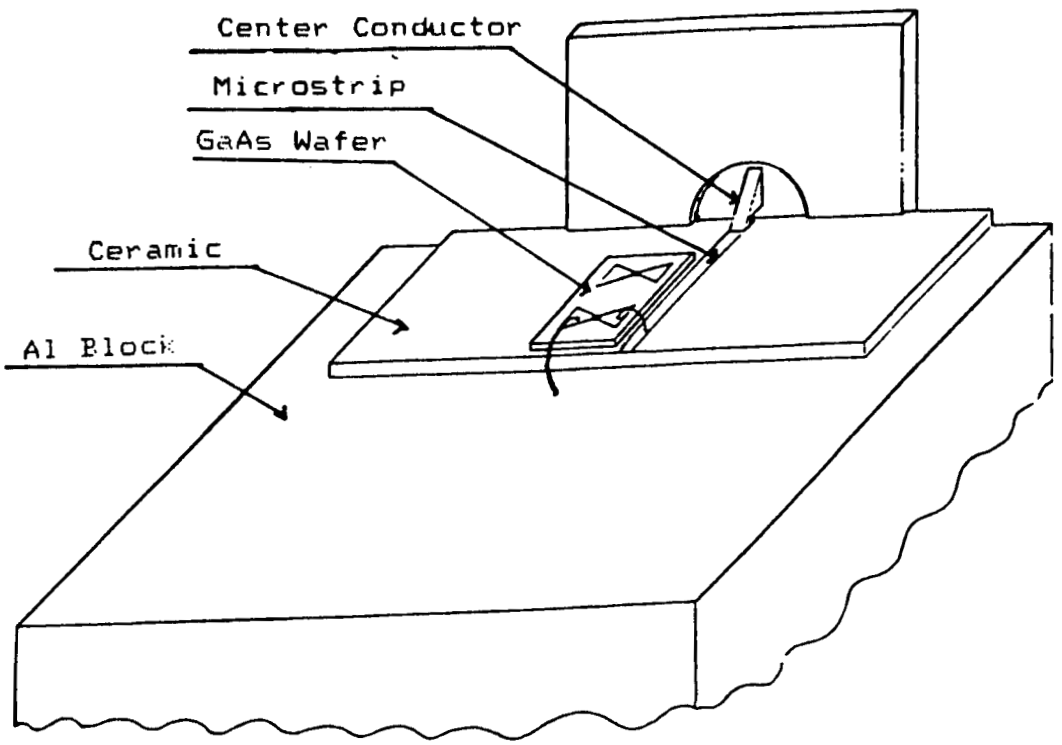


Fig. 2.7. Mounting of detectors on Al block.

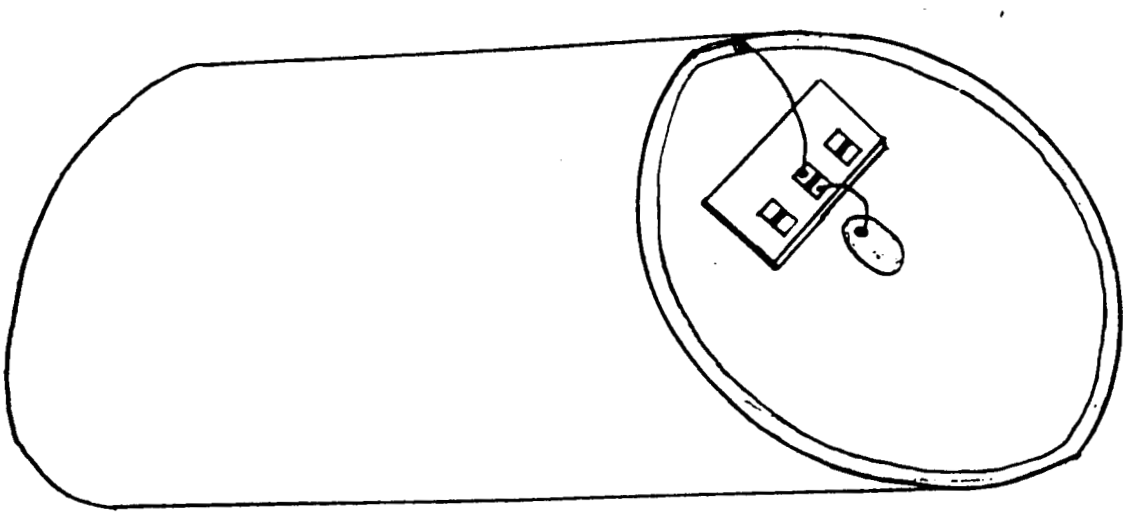

Fig. 2.8. Mounting of detectors on semi-rigid coax.

## 2.12 CONCLUSIONS

In this chapter some properties of the structure, on which the detectors were fabricated, were presented along with the actual fabrication process. The different geometries of the detectors to be characterized were also presented. Finally, the methods of mounting and bonding the detectors for testing purposes were explained. The next chapter will deal with some of the actual measurements on the detectors, namely, frequency response and responsivity.

# CHAPTER 3

# FREQUENCY RESPONSE AND GAIN OF DETECTORS

## 3.1 INTRODUCTION

Perhaps the most important characteristic to a MMIC designer who wishes to incorporate a photodetector is the detector's frequency response. The frequency response of the detector reveals two important factors; 1) what frequency the response is flat up to and 2) what is the highest frequency at which usable gain exists. These two parameters can determine whether detector is applicable to the designer's needs. Another parameter which may be of concern is the detector's responsivity. By knowing the responsivity of the detector the designer can determine whether the detector is appropriate for use with the current light source.

In this chapter both the frequency response to modulated light and the responsivity of the various detectors will be measured along with an analysis of each. A brief discussion of the photoconductive operation of the detectors will also be presented. Quantum efficiencies, both internal and external, of the detectors will be calculated from the responsivity measurements.

## 3.2 THEORY OF OPERATION

The detectors reported in this work are planar photoconductors on a HEMT structure. An interdigitated geometry is used to effectively increase the active area while keeping electrode spacing small. The incident light (0.82 μm) is such that the AlGaAs window is essentially transparent to it. Light of this wavelength has an absorption depth of approximately 1 μm in GaAs [45] and therefore most of the absorption occurs within the undoped layer of GaAs. The incident photons generate electron hole pairs, of which the electrons diffuse toward the 2DEG and the holes are forced away by the band bending. The applied DC bias creates a lateral field leading to the creation of a photocurrent.

Photoconductivity is a relatively complex phenomenon which rarely permits a closed form solution incorporating all the contributing factors, such as trapping, non-uniform samples, surface reflections, angle of incident light, temperature, etc. Only a simple solution will be presented here, as the purpose is to report observed results and others have already provided extensive analysis of the photoconductive process [46-49].

If trapping effects are neglecting then the photocurrent density, J, may be written as

$$J = qGt_{eff}(\mu_n + \mu_p)E \qquad (3\text{-}1)$$

where q is the electron charge, G the electron-hole generation rate, $t_{eff}$ the effective carrier lifetime, E the electric field and $\mu_n$, $\mu_p$ the mobility of electrons and holes [48]. This may be

alternately written as a photoconductive current $I_p$

$$I_p = qn\Phi A \qquad (3\text{-}2)$$

where q is the electron charge, n the quantum efficiency, $\Phi$ the photon flux, and A the effective illuminated area [50].

One of the inherent properties of photoconductors is their ability to achieve internal gain. The dynamic gain, G(w), is defined as the ratio of the number of electrons collected at load to the number of incident photons in the active area. It can be expressed as

$$G(w) = t_{eff}/t_t \times [\ (1-e^{-aW})/(1 + jwt_{eff})\ ] \qquad (3\text{-}3)$$

where w is the frequency in rad/sec, $t_{eff}$ is the effective lifetime, $t_t$ the transit time, a the absorption length and W the active layer depth [51]. The above equation is for the trap free case and $t_{eff}$ can be calculated as follows:

$$1/t_{eff} = 1/t_o + 1/t_c + 1/t_s \qquad (3\text{-}4)$$

where $t_o$ is the bulk carrier lifetime, $t_c$ the lifetime determined by recombination at the contacts, and $t_s$ determined by surface recombination. The relative contributions of $t_c$ and $t_s$ depend on the geometry of the device. This leads to a simple pole at $w = 1/t_{eff}$ with a roll off of 20 dB/decade.

The above discussion has ignored two factors which can greatly affect detector bandwidth, namely the dielectric relaxation time, $t_r$, and the effects of trapping. In devices which have extremely low dark currents the dielectric relaxation time may limit the cutoff frequency of the detectors [46]. For the case of $t_{eff} >> t_r$ the result is the single pole at $1/t_{eff}$ as

above. When $t_r >> t_{eff}$, however, the primary pole is at $1/t_r$ and the response will fall to a plateau and remain flat until a secondary pole at $1/t_{eff}$ will induce further roll-off.

Traps may be unintentionally created in the fabrication process, e.g., the outdiffusion of Cr from semi-insulating GaAs substrates [48]. Trapping is common in photoconductive detectors and is identified by a long tail after excitation by a short pulse [48-51]. Trapping leads to an effective electron lifetime of:

$$t_n = t_o \left[ 1 + \sum_i \frac{(N_i - p_i)c_{p\,i}}{(p_o c_{p\,i} + e_{p\,i} + jw)} \right], \qquad (3\text{-}5)$$

where the sum is over i discrete trapping levels. $t_{eff}$ is now controlled by the capture rates, $c_{p\,i}$, the emission rates, $e_{p\,i}$, the hole concentration, $p_o$, and the trapping center density $N_{t\,i}$ [50,51]. Because of the numerous hole trapping levels due to lattice defects and contamination the response will show an almost continuous decrease from CW. This roll-off will not necessarily follow the standard 20 dB/decade due to the complexity of switching from one trapping level to the next [50]. The roll-off instead tends to be between 10 and 15 dB/decade.

## 3.3 MEASUREMENT SYSTEM

A physical and electrical schematic representation of the system used to make frequency response measurements are given in Figures 3.1 and 3.2 respectively. The mounted detector is connected to a bias tee via a SMA connector, which is in turn connected to a SMA tee providing the 50 ohm load. The rf signal is carried on microwave coax from the SMA tee to a wide band amplifier (Avantek 2.0-18.0 GHz and Avantek 0.01-2.1 GHz) to an HP 8566A spectrum analyzer. The spectrum analyzer has two frequency ranges (0-2 GHz and 2-22 GHz) and was used to make all frequency response measurements.

The light modulation is provided by an Ortel TSL-1000 Laser Diode ( $\lambda$ = 0.82 μm) driven by an HP 8350B sweep oscillator. The light is carried by a single mode optical fiber which is then positioned over the detector by means of a x,y,z translation stage. The linearity of both the sweep generator and laser were confirmed by the use of known high speed detectors (Ortel RSL-25). The complete system exhibits a single pole at about 2.5 GHz and multiple poles beyond 10 GHz (see Fig. 3.3).

The entire system is controlled by means of a HP 9836C computer. The sweep oscillator and spectrum analyzer are remotely controlled by means of the GPIB ports. The computer also allows the combination of the two frequency ranges as the entire range can not be swept at one time.

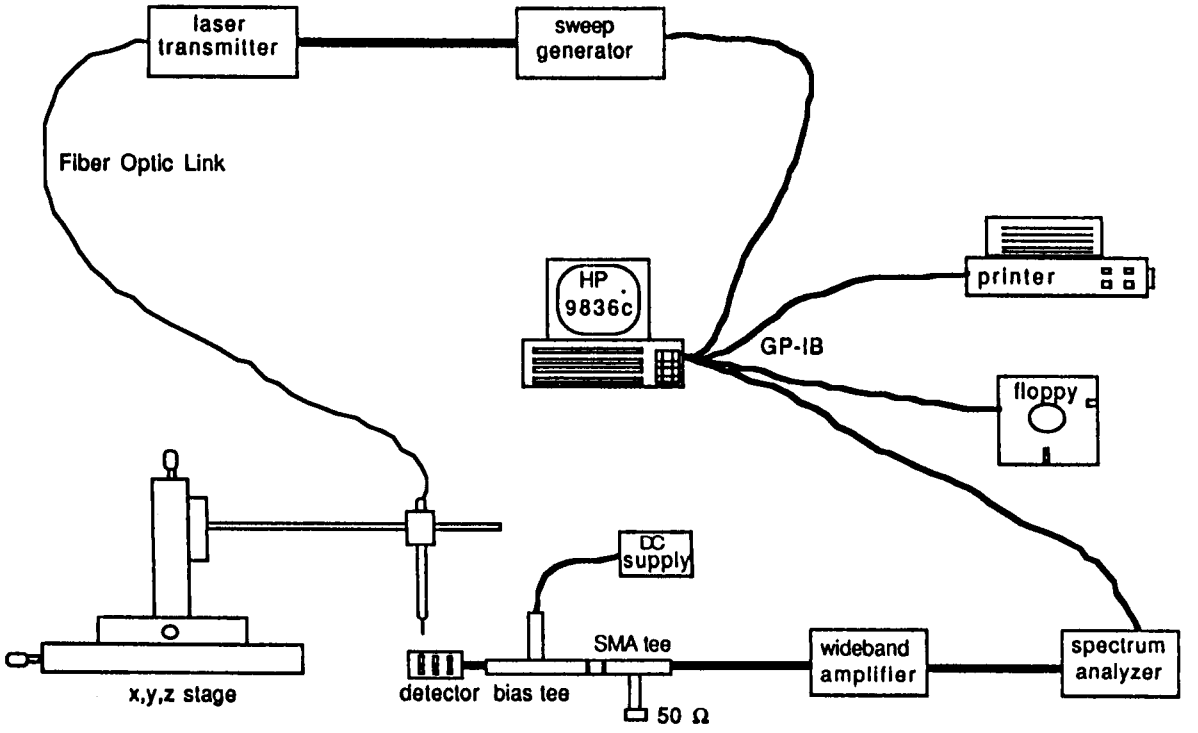


Fig. 3.1. Physical representation of measurement system.

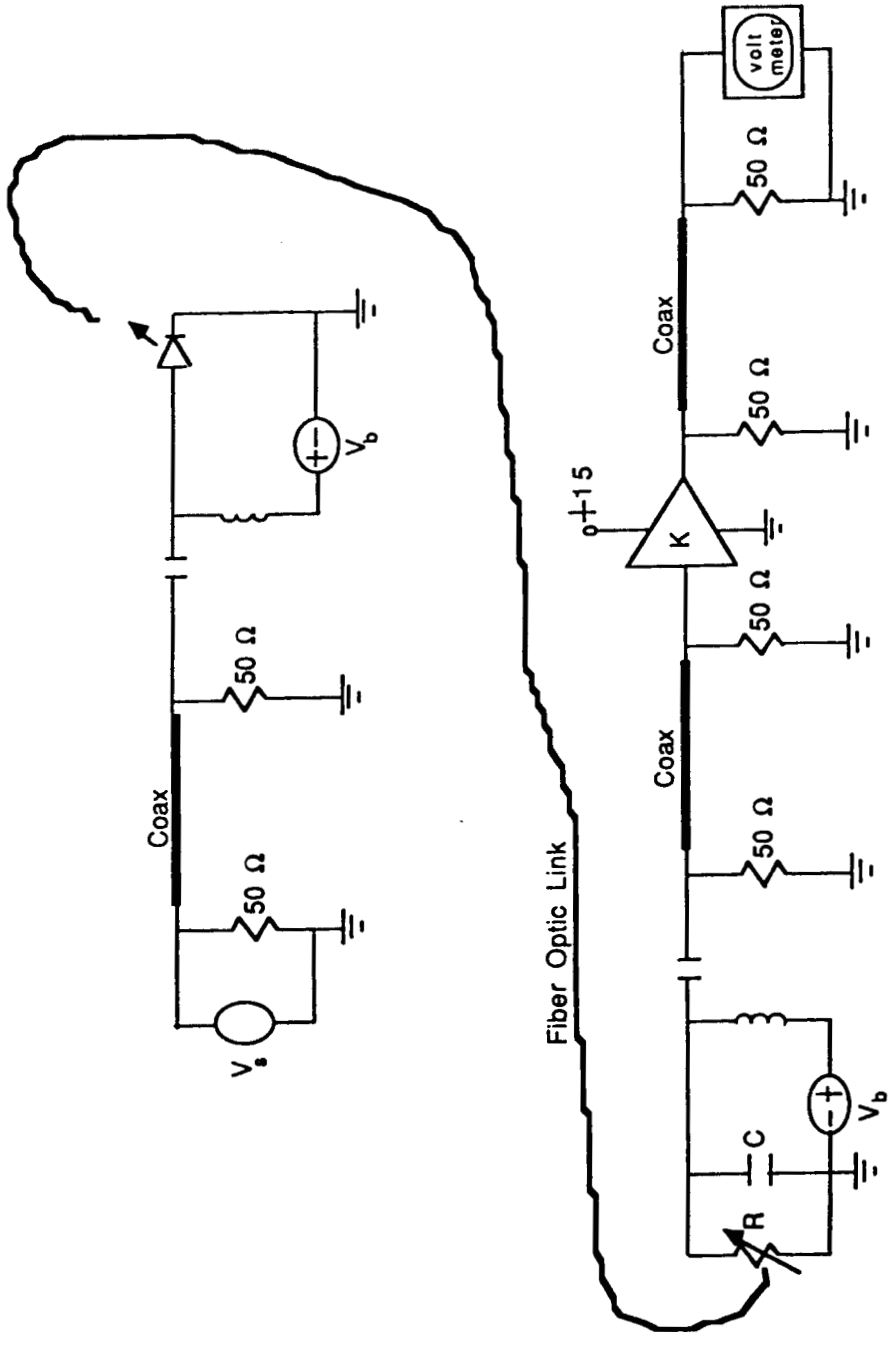


Fig. 3.2. Electrical representation of measurement system.

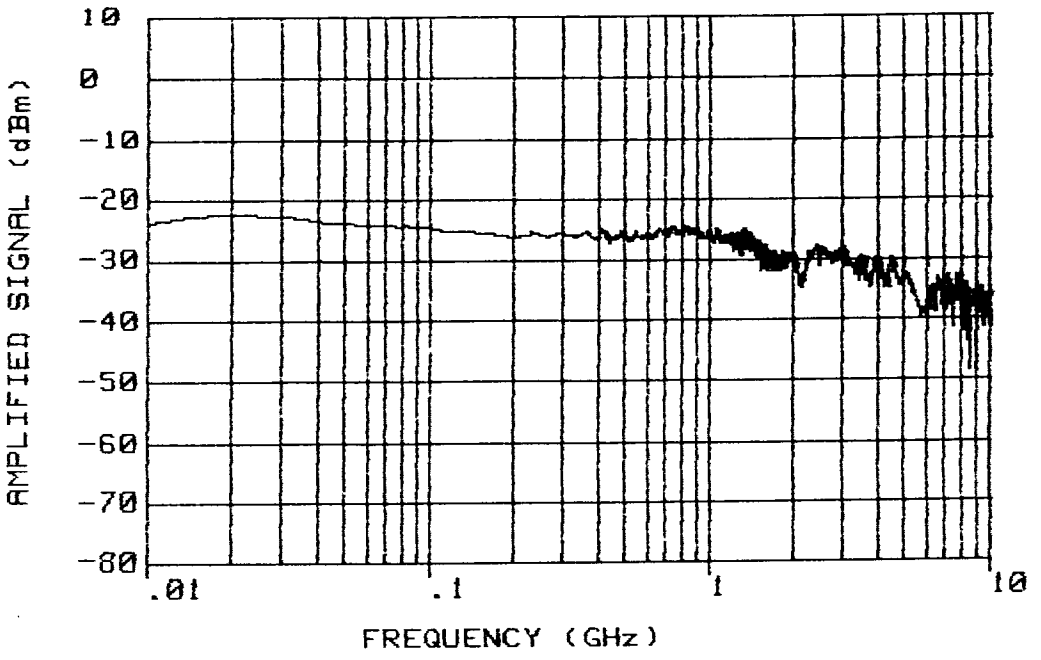


Fig. 3.3. System frequency response.

## 3.4 ALIGNMENT AND MEASUREMENT TECHNIQUE

The alignment procedure is fairly simple if a little crude. The detector to be tested is connected to the SMA tee with the tee's bias input connected to a Tektronix 576 curve tracer. The end of the optical fiber is then "eye-balled" over the detector by means of the x,y,z translation stage. The rf output of the sweep oscillator is set to 500 MHz and enabled. Position adjustment of the fiber is made until the lowest DC resistance is obtained (greatest slope on curve tracer). Note that the power level on the curve tracer must be kept low ( <2 mW) in order to prevent damaging the detector's fingers.

If desired, further alignment adjustment may be made by connecting the DC bias-tee to a DC power supply (0 - 1.0 V). The coax to the wide band amplifier is reconnected and the spectrum analyzer set to detect the desired frequency. The x,y,z stage is further adjusted such that the highest signal strength is achieved. This additional procedure normally results in very minute adjustments, if any at all, to those done with the curve tracer.

Frequency response measurements were made using the program "response" (see Appendix A). The program prompts the user for desired start and stop frequencies as well as the output power level of the sweep oscillator. The program then sets up the sweep oscillator and spectrum analyzer accordingly. The input frequency range is single stepped through the specified range in 500 equal steps. The entire frequency range is scanned three

times and then averaged to obtain the final response.

## 3.5 FREQUENCY RESPONSE MEASUREMENTS

The measured frequency response of three different detector geometries is shown in Fig. 3.4. The response characteristics of the three detectors are nearly identical with only absolute gain differing by a constant offset. Measurements performed on all five detector geometries with a lower bandwidth laser also resulted in no difference in response with electrode geometry.

The detectors all exhibit a 3dB cutoff frequency of approximately 185 MHz. The gain then decays at 12 dB/decade in the decade between 100 MHz and 1 GHz with a small plateau at 510 MHz and a larger one at 1 GHz. The response falls off at the normal 20 dB/decade after the 1 GHz plateau. The deviation from the normal 20 dB/decade slope and presence of gain plateaus would seem to indicate the presence of trapping.

No equipment was available for making time domain measurements and therefore the presence of the characteristic long tail cannot be checked for. Others [35], however, have done a time analysis on detectors on an identical material but larger geometry (5 μm spacing). Their pulse response exhibited the long optical tail and their calculated 3 dB frequency of 170 MHz agrees well with the measured value of 185 MHz. In addition, Papaioannou et. al. [51] have discussed the effects of minority trapping and have shown a 12 dB/decade slope between 100 MHz and 1 GHz for a planar photoconductor. The plateau at 510 MHz is most likely due to a discrete trapping level, whereas the 1 GHz

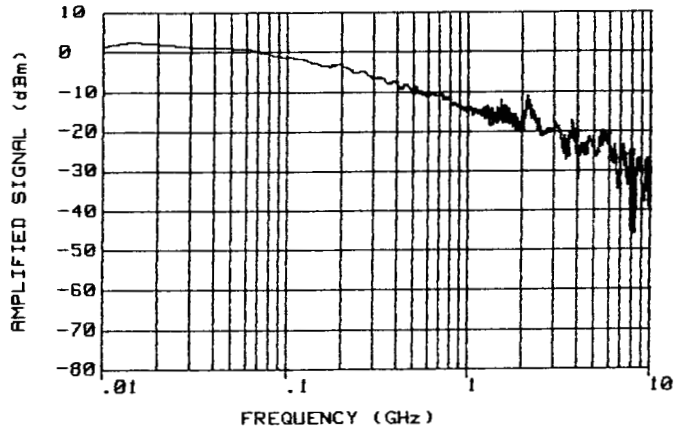


a. Frequency response of 1 x 1 μm detector.

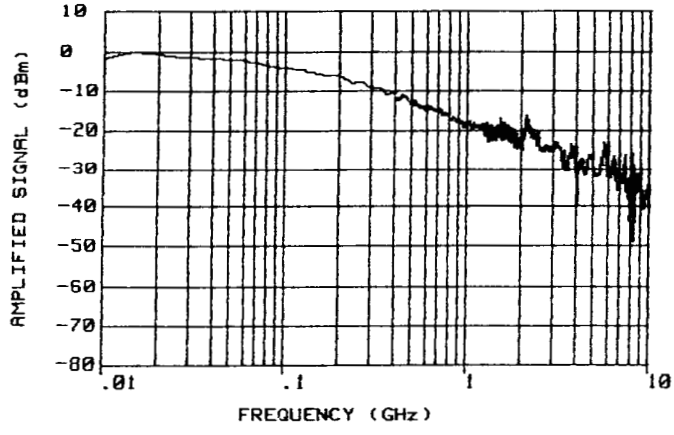


b. Frequency response of 2 x 2 μm detector.

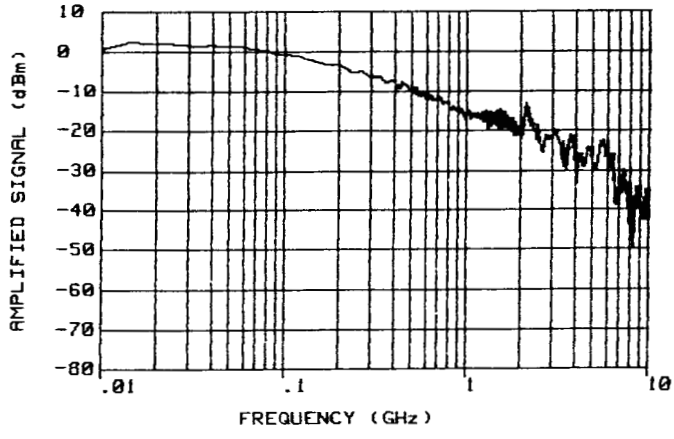


c. Frequency response of 2 x 3 μm detector.

Fig. 3.4. Frequency response of interdigitated detectors.

plateau is attributed to entering the trap-free regime [50,51]. This would indicate a trap-free cut-off frequency of approximately 2 GHz.

For the sake of comparison the response of some simple straight gap photoconductors was also measured. Fig. 3.5 shows the results of these measurements. These detectors are fairly flat ($\pm$ 0.7 dB) until a 3 dB frequency of 385 MHz. The reason for the absence of the trapping seen in the interdigitated detectors is unknown but the response shows that the detectors are definitely not transit time limited as the gap is much larger for these detectors (10 μm, 20 μm and 50 μm).

### 3.6 RESPONSIVITY MEASUREMENTS

Responsivity measurements were made using an Ortel SL620 laser. This laser permits the output optical power to varied while being monitored by an internal photodiode with a voltage proportional to the optical power. The output voltage from the photodiode was then calibrated against the actual optical power by means of a digital power meter. Responsivity measurements were made at 500 MHz and 1 volt bias unless otherwise stated.

As a reference for the measurements the responsivity of a p.i.n. diode, with an external quantum efficiency of 55%, was measured (see Fig. 3.6). This plot indicated a responsivity of 0.33 A/W which is in excellent agreement with the specified (0.3-0.35 A/W) responsivity. The quantum efficiency is directly proportional to responsivity [50] as seen by

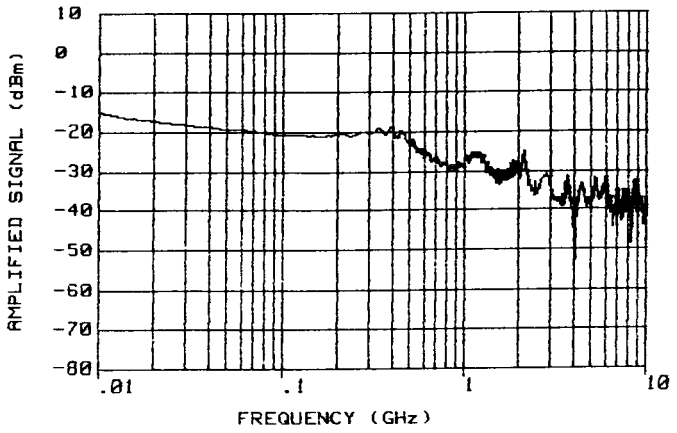


a. Frequency response of 10 μm gap detector.

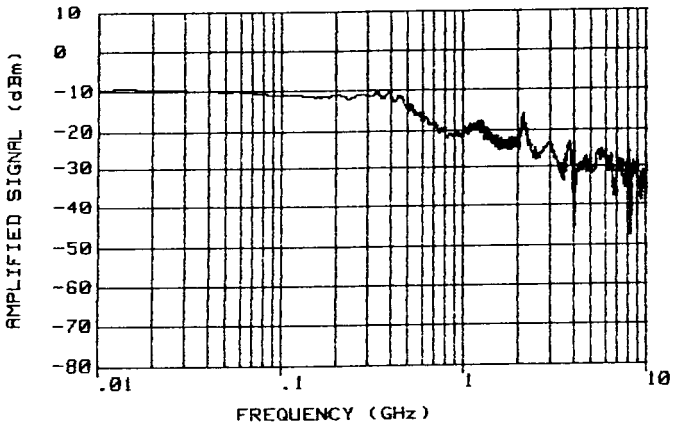


b. Frequency response of 20 μm gap detector.

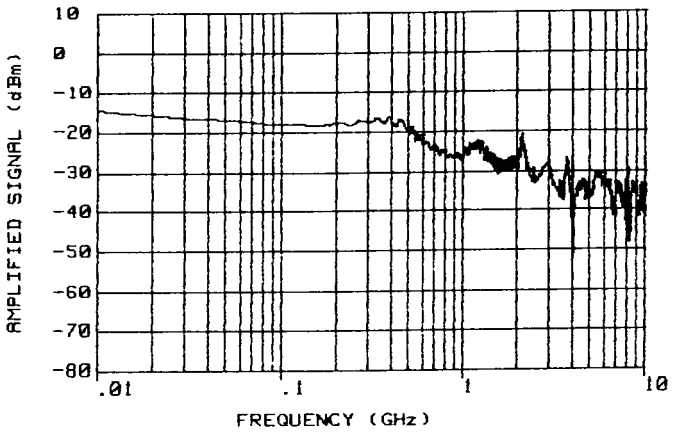


c. Frequency response of 50 μm gap detector.

Fig. 3.5. Frequency response of gap detectors.

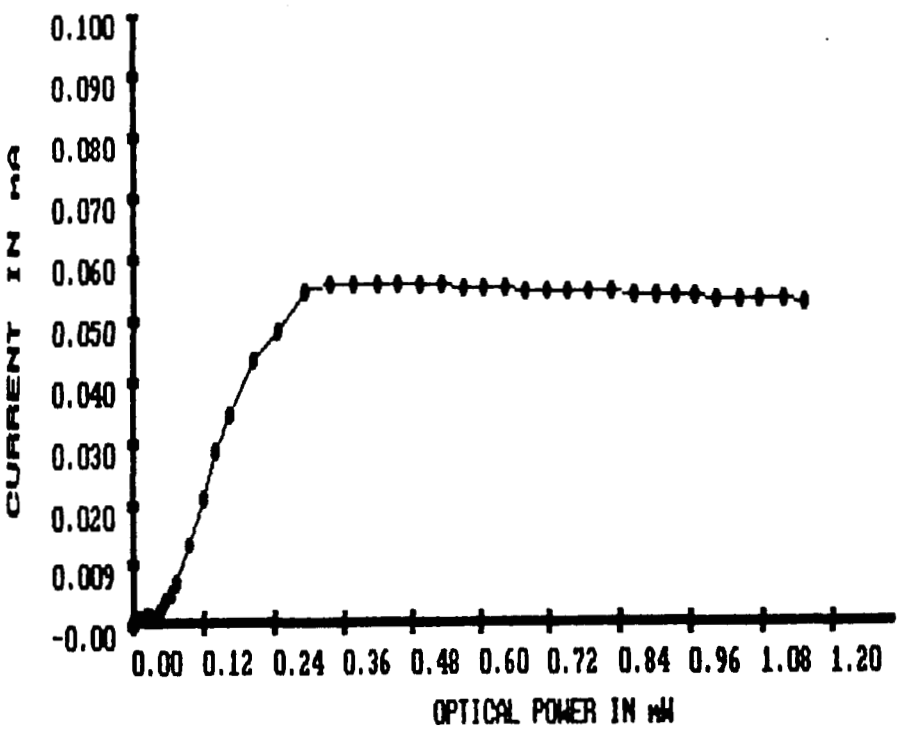


Fig. 3.6. Responsivity of reference PIN detector.

$$R_o = qn(1-r)/hv \qquad (3\text{-}6)$$

where q is the electron charge, r is the reflection coefficient, h is Planck's constant and v the frequency of the incident light. Assuming the p.i.n. diode has an antireflection coating this formula agrees extremely well with the measured value. For Group III-V compounds without an antireflection coating the air-to-semiconductor reflection coefficient is 0.3 [52], this leads to a reduced formula of:

$$R_o = 0.46 \times n. \qquad (3\text{-}7)$$

The responsivity values presented for the detectors should not necessarily be considered nominal values but minimum values. This is due to the fact that it is not possible to insure that the detector surface and fiber optic end are precisely normal to one another. In addition these detectors are not packaged in any way and therefore, may suffer from surface contamination. Variation in responsivity for identical detectors can be seen in Fig. 3.7. Fig. 3.8 shows the responsivity plots for other detector geometries.

These figures relate to peak responsivities from 0.13 A/W to 0.31 A/W. The responsivity was measured as the slope of the graph in its most linear region (typically between 50 μW and 200 μW). Responsivity is known to follow the same dependence on frequency that the gain does [50]:

$$R(w) = R_o/(1 + jwt_{...}).$$

Taking into account the frequency response of the responsivity

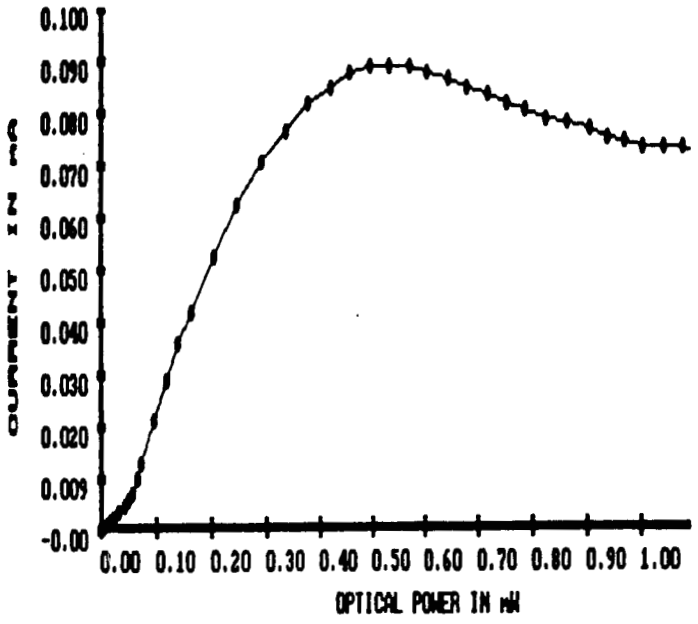


Detector A: Responsivity = 0.31 A/W.

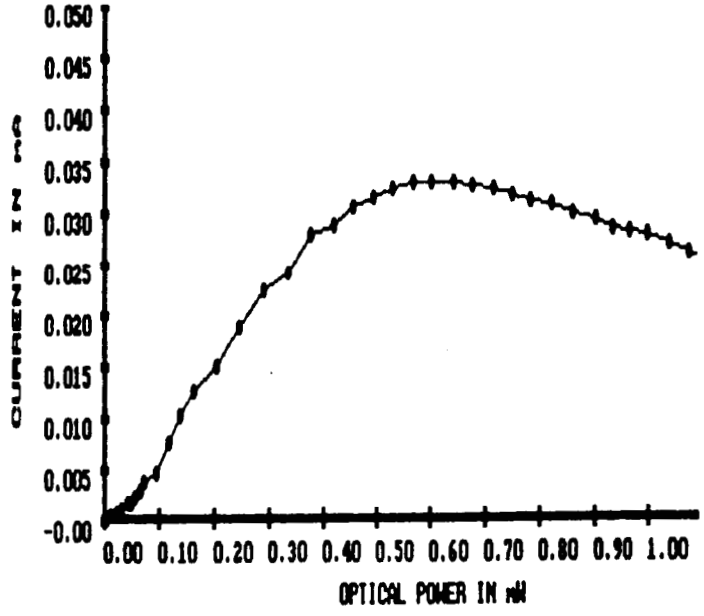


Detector B: Responsivity = 0.10 A/W.

Fig. 3.7. Response of two detectors of same geometry

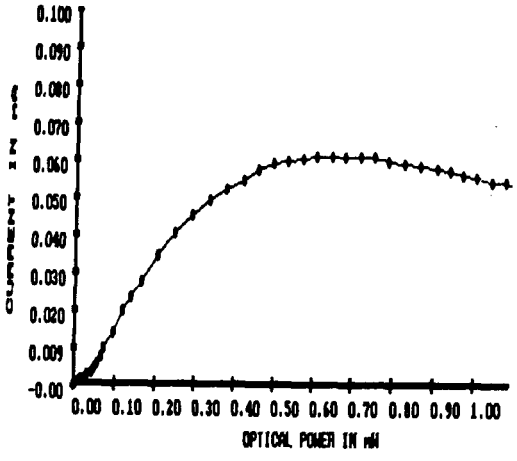


a. Response of 1 μm x 1 μm detector.
(Responsivity = 0.21 A/W.)

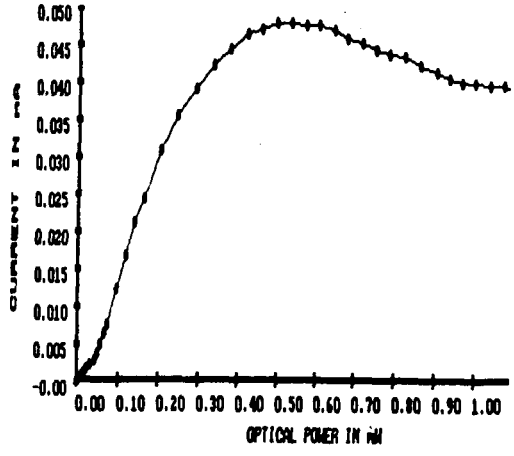


b. Response of 2 μm x 2 μm detector.
(Responsivity = 0.18 A/W.)

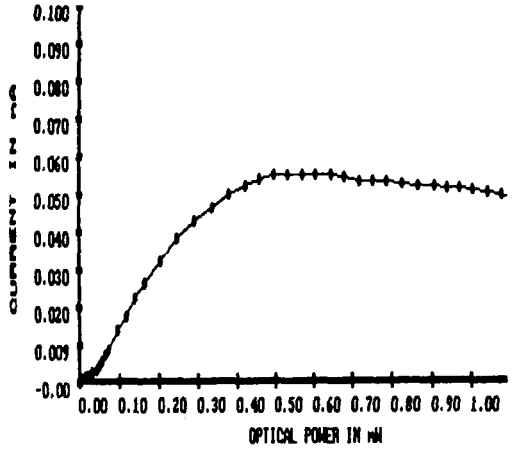


c. Response of 2 μm x 3 μm detector.
(Responsivity = 0.22 A/W.)

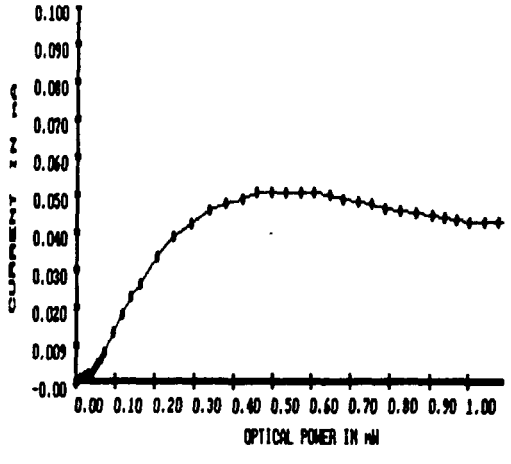


d. Response of 2 μm x 4 μm detector.
(Responsivity = 0.22 A/W.)

Fig. 3.8. Detector responses and responsivities.

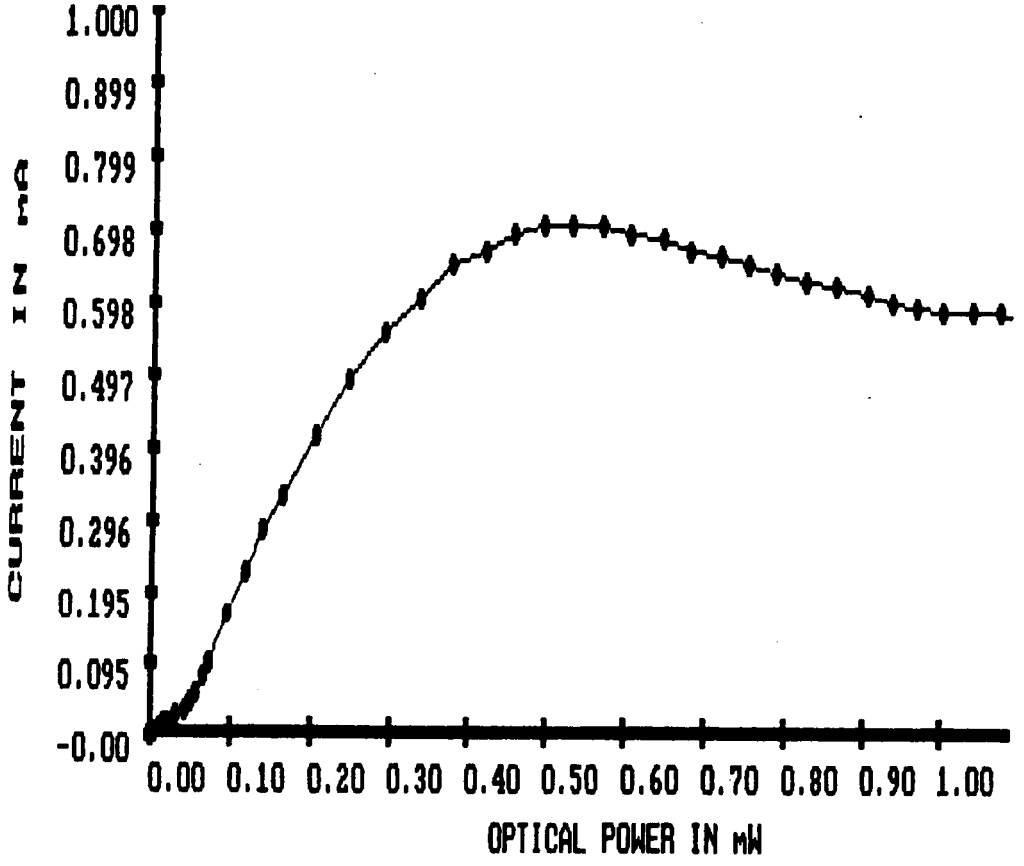


Fig. 3.9. Adjusted response of 1 μm x 1 μm detector.

this leads to an adjusted responsivity of 2.5 A/W for the 1 x 1 μm detector (see Fig. 3.9). A responsivity of 2.5 A/W translates into a quantum efficiency, n, of 5.44. This n is the value which would be possible to achieve if an anti-reflection coating was used; as such coatings can reduce the reflection coefficient from 30% to below 1% [53]. For the 1 x 1 μm detector it represents an external quantum efficiency of 3.81 which is comparable with that found in GaAs detectors.

## 3.7 CONCLUSIONS

In this chapter the frequency response of the detectors to modulated light was presented. It was shown that the detectors' response was independent of interelectrode geometry and therefore not transit time limited. It was proposed that the poor response of the detectors was due to minority carrier trapping rather than an RC time constant or large dielectric relaxation time. Trapping was suspected because of the non-standard 12 dB/decade roll-off whereas an RC time constant or large dielectric relaxation time would result in the standard 20 dB/decade roll-off. The interdigitated detectors did exhibit a 3 dB bandwidth of 185 MHz which is comparable to that of GaAs detectors.

Quantum efficiency calculations were also made from the measured responsivity of the detectors. An external quantum efficiency of 3.81 was calculated for a 1 x 1 μm detector. This quantum efficiency with the measured bandwidth of 185 MHz yields a gain-bandwidth product of 705 MHz.

It is believed that the performance of these detectors could

be enhanced in a number of ways. The responsivity of the detectors could be increased by as much as 30% by applying an antireflection coating to the surface of the detectors. This would relate to a corresponding 30% increase in the external quantum efficiency and therefore gain-bandwidth product.

The bandwidth of the detectors could also possibly be expanded in a number of ways. The first method would be the use of "back-gating" to sink the minority hole carriers and reduce the effects of trapping. The second method would require the growth of a new structure which would have a thin layer of AlGaAs between the semi-insulating substrate and the undoped GaAs in order to prevent the outdiffusion of contaminants which might lead to trapping.

The next chapter will deal with the impedance properties of the detectors which is also of importance to the designer of MMIC devices.

# CHAPTER 4

# IMPEDANCE PROPERTIES OF PHOTOCONDUCTORS

## 4.1 INTRODUCTION

Knowing the electrical impedance of the detectors is very useful for photoreceiver design. If the impedance is known it becomes possible to match the impedance of the detector with that of the amplifier to achieve maximum power transfer. Many detectors, both photodiodes and photoconductors, exhibit RC time constant limited response. In many cases equalization can greatly improve the response characteristics of the detectors. The input impedance of the amplifier stage may be designed so as to "equalize" the effects of the parasitic capacitances and inductances. Chen et. al. [28] have demonstrated an improvement in frequency response from 60 MHz to >1 GHz by means of a simple parallel RC equalizer.

In this chapter both the DC and AC impedance characteristics of the various detectors will be examined. The AC characteristics will be determined from $S_{11}$ parameter measurements as the detectors are symmetrical two terminal devices. A corresponding small signal model will also be developed to explain the detectors' behavior.

## 4.2 DC CHARACTERISTICS

Typical DC I-V curves for three detectors are shown in Fig. 4.1. The curves show that the detectors are symmetric devices whose operation is independent of bias polarity. The resistance of the detectors is linear for small bias and smoothly increases as bias is increased until it becomes quite large. The shape of these I-V curves is very similar to those reported by others [30,35,55] and is very similar to that of ungated GaAs FET's [54]. The flattening of the curve is due to carrier velocity saturation at the higher fields.

The effect of increasing optical power on the DC impedance is also shown in Fig. 4.1. The detectors were illuminated with white light from a variable intensity microscope lamp. As the intensity was increased the resistance correspondingly decreased. The 1 x 1 μm detectors exhibit a much lower resistance than the 2 x 2 μm and 2 x 3 μm detectors. This is due to their smaller interelectrode spacing. The 2 x 2 μm and 2 x 3 μm show nearly the same response to variations in light. This intuitively makes sense because the 2 x 2 μm detectors' interelectrode spacing is 1.5 times less than the 2 x 3 μm detectors' but the 2 x 3 μm detectors posses 1.5 times the absorption area.

Dark field measurements made on the detectors yield a dark current below 1 μA. The measurements were limited by the sensitivity of the curve tracer, which has a lower limit of 1 μA for current measurements.

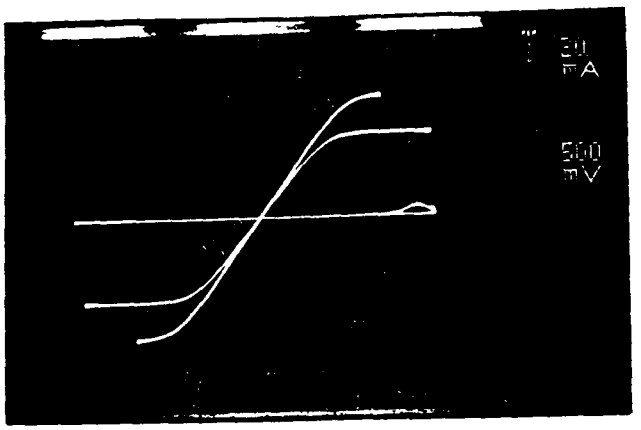


a. Effect of increasing illumination on I-V characteristic of 1 μm x 1 μm detector.

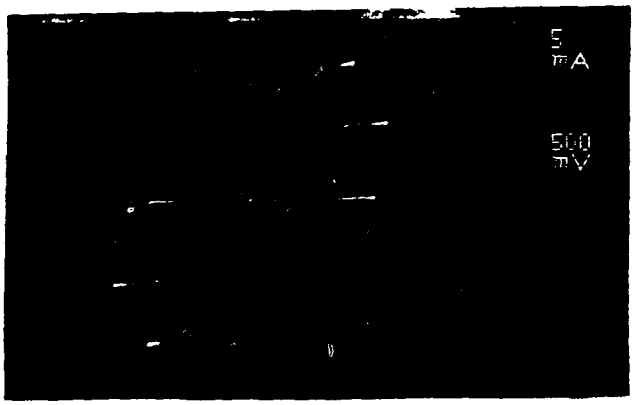


b. Effect of increasing illumination on I-V characteristic of 2 μm x 2 μm detector.

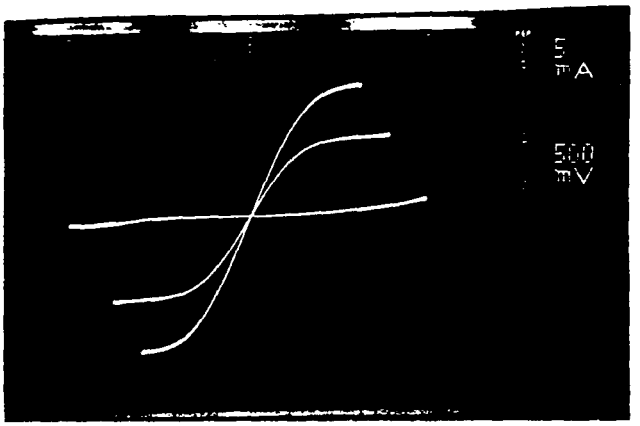


b. Effect of increasing illumination on I-V characteristic of 2 μm x 2 μm detector.

Fig. 4.1. Effect of illumination on detector I-V characteristics

## 4.3 S-PARAMETER MEASUREMENTS

In order to properly model the AC characteristics of the detectors it was necessary to make impedance measurements at high frequency with varying bias and light intensity. To this end reflection coefficient, $S_{11}$, measurements were made under various conditions. $S_{11}$ measurements were made on similar detectors mounted using both methods (see Fig. 4.2), but because of problems with properly modeling the microstrip transmission line only those mounted on the semi-rigid coax will be discussed.

The measurements were made with an HP-4910 Network Analyzer using the arrangement shown in Fig. 4.3. The frequency was swept from 0.5 GHz to 5.5 GHz. The lower frequency bound being determined by the limitations of the network analyzer and the upper bound by the frequency range permissible for modeling purposes. Calibration procedures are such that it proved impossible to orient the reference plane at the detector, but rather at the end of the Bias Tee. The $S_{11}$ parameters of Fig. 4.2 therefore include the effects of the coax cable. These plots provide little useful information in their raw form, but by using an CAE package [56] and proper modeling of the coaxial cable [57] it was possible to find the true response of the detectors and develop a corresponding model.

Fig. 4.4 shows the variation of $S_{11}$ measurements with incident light intensity, with the effects of the coax cable removed. These plots demonstrate how the resistance of the detectors decreases with increasing light intensity. The value of the AC

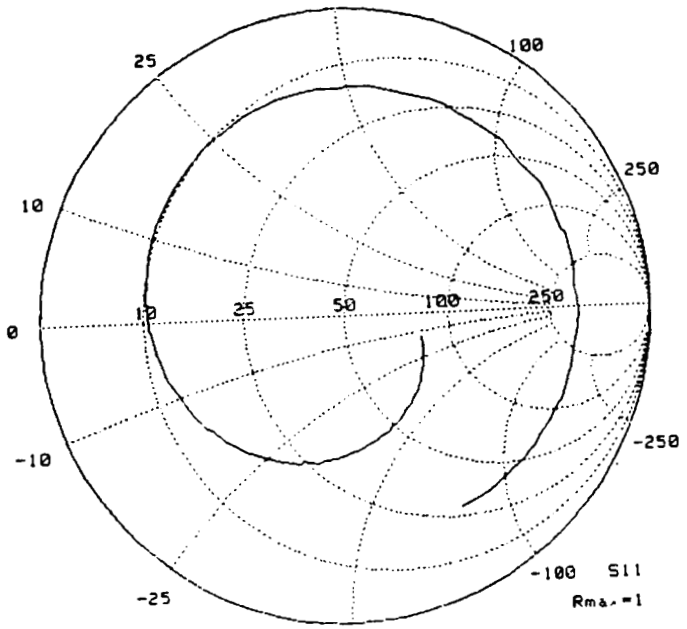


a. $S_{11}$ of detector mounted on Al block.

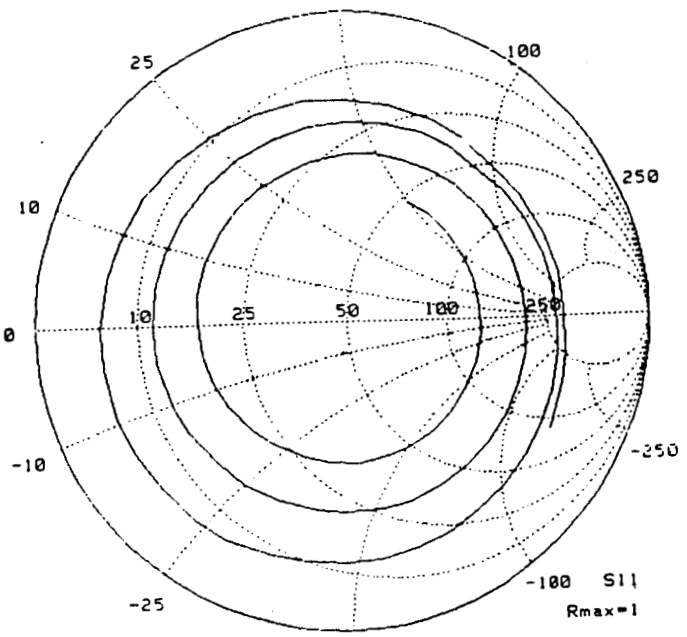


b. $S_{11}$ of detector mounted on rigid coax.

Fig. 4.2. Effect of mounting on $S_{11}$.

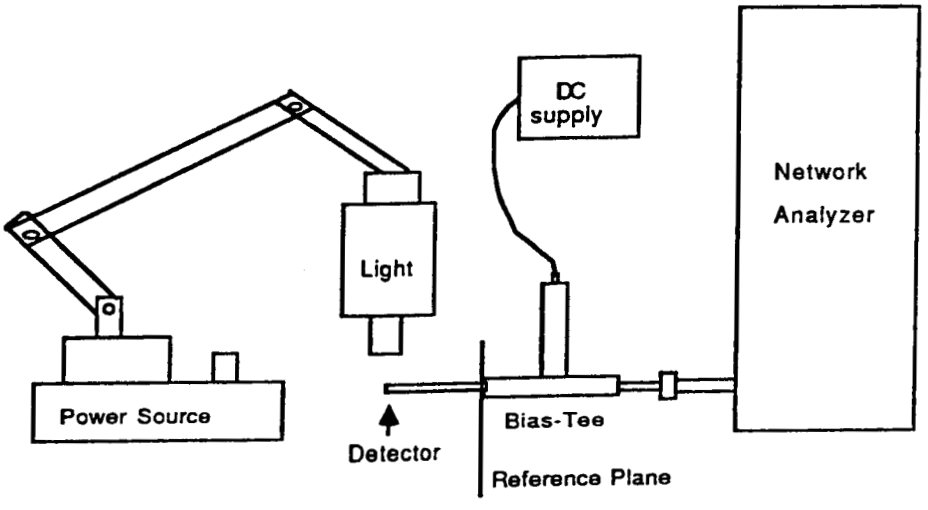


Fig. 4.3. Impedance measuring system.

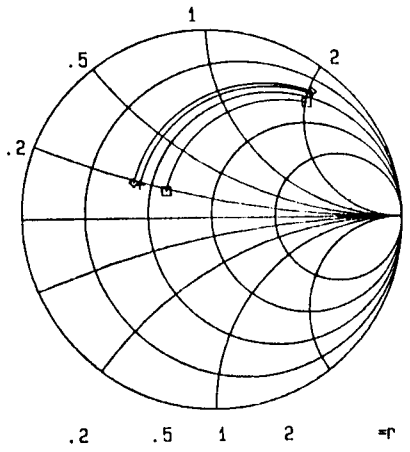


Ambient light
1st level light
2nd level light

a. Effect on 1 μm x 1 μm detector.

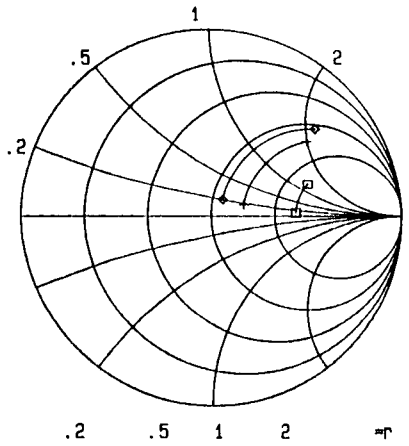


Ambient light
1st level light
2nd level light

b. Effect on 2 μm x μm detector.

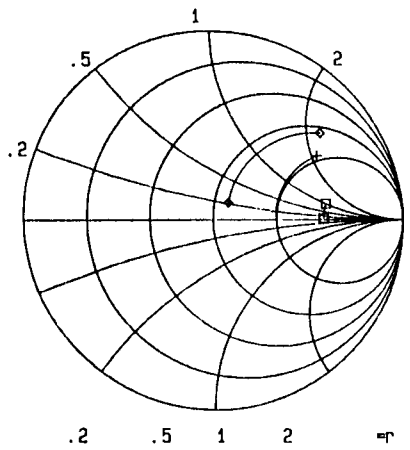


Ambient light
1st level light
2nd level light

c. Effect on 2 μm x 3 μm detector.

Fig. 4.4. Effect of illumination level on $S_{11}$.

resistance is in fact in very good agreement with the DC value obtained from the I-V curves. Fig. 4.5 shows the effect of increasing DC bias on input impedance. The resistive component drastically increases as the bias is increased to above the knee in the I-V curves, so that the impedance eventually becomes capacitive. Fig. 4.6 demonstrates the variation in impedance with interelectrode geometries. This also follows a pattern very similar to that seen in the DC characteristics.

## 4.4 SMALL SIGNAL MODEL

In order to arrive at a small signal model for the detectors the above mentioned CAE package was used, and the modeled $S_{11}$ values were compared to the actual $S_{11}$ measured values over the given frequency range. Circuit parameters were varied to minimize the least square error between the calculated and measured values. The least square error in the fit is between 0.002 and 0.003 over the measured frequency range. The model that was developed is shown in Fig. 4.7 and consists of a parallel RC combination with an inductance in series with each node of the RC network. The inductance is due in part to the bonding wire and in part to a parasitic inductance associated with the electrodes. This model is similar to that developed by Wojtczuk [55] and leads to a complex impedance given as follows:

$$Z = \{R/[1 + (jwRC)^2]\} + j\{w(L_1 + L_2) - wCR^2/[1 + (wRC)^2]\} \qquad (5\text{-}1)$$

Varying the light intensity affects each of the components of the model differently. The effect on R, which drops from well over 100 Ohms at ambient light to only a few tens of Ohms at the

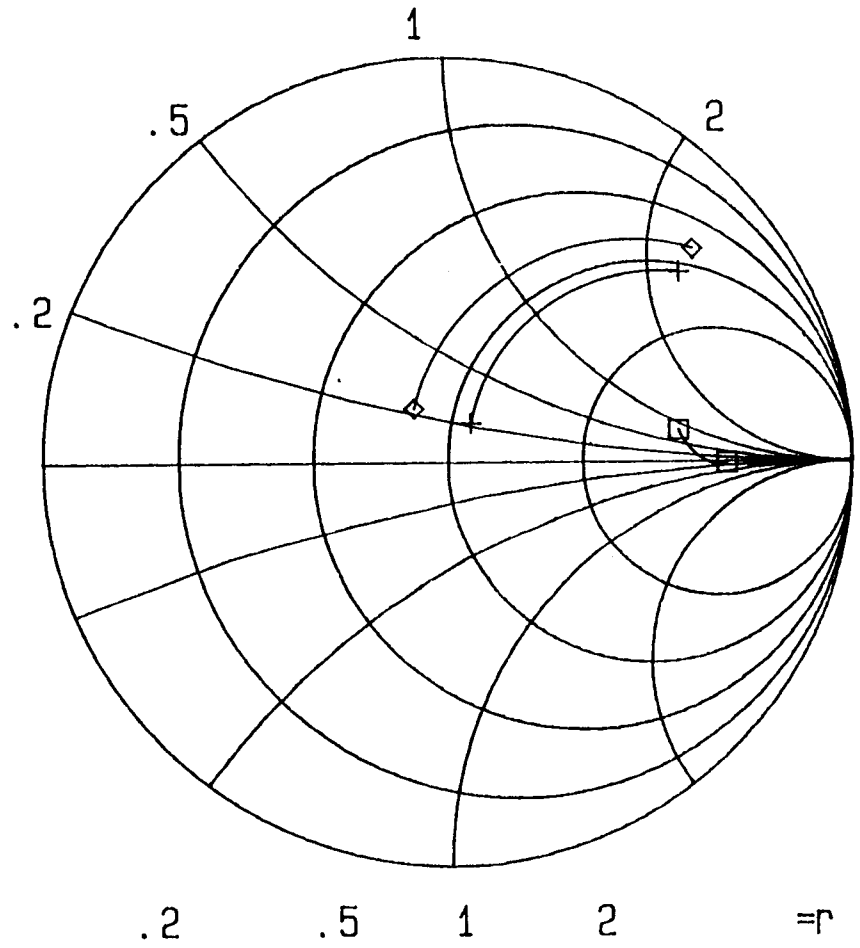


Bias = 0.0 V

Bias = 1.0 V

Bias = 3.0 V

Fig. 4.5. Effect of bias voltage on $S_{11}$.

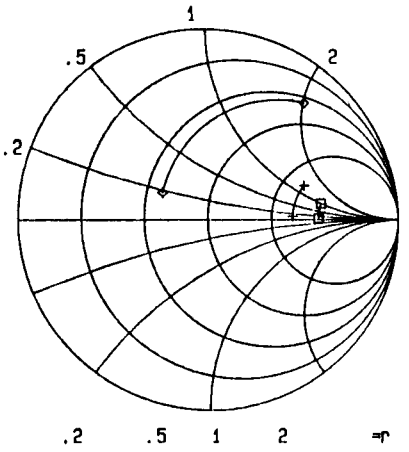


1 x 1 μm detector
2 x 2 μm detector
2 x 3 μm detector

a. Ambient light

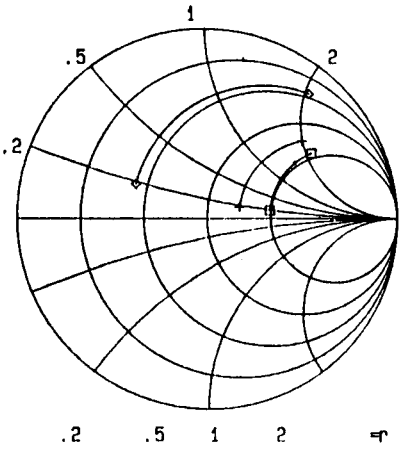


1 x 1 μm detector
2 x 2 μm detector
2 x 3 μm detector

b. 1st level light.

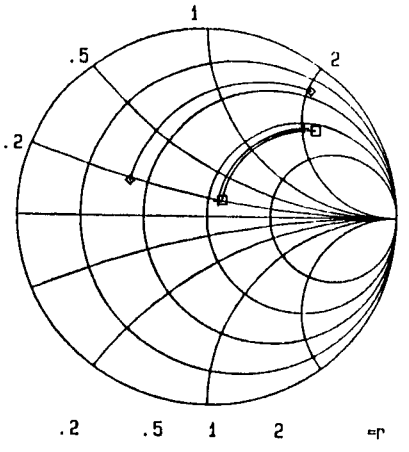


1 x 1 μm detector
2 x 2 μm detector
2 x 3 μm detector

c. 2nd level light.

Fig. 4.6. Effect of illumination on $S_{11}$.

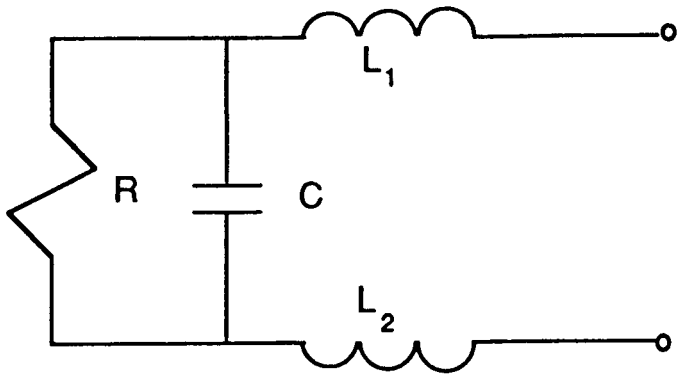


a. Small signal model.

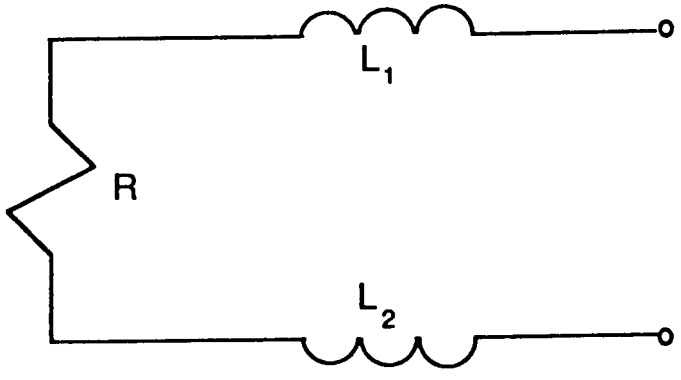


b. Low bias equivalent circuit.

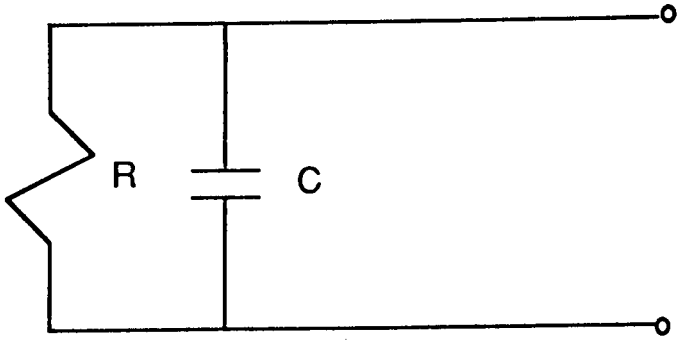


c. High bias equivalent circuit.

Fig. 4.7. Detector equivalent circuit under various conditions.

high intensity setting, is the most notable. This large change in resistance has been observed by others [58] but only at low bias while at high bias they observed little or no change. In this work it was observed at all bias conditions tested. The effect is expected and is due to the addition of the photoconductive current, in effect lowering the resistance of the detector. At higher bias conditions the resistance should still decrease with increased light but the magnitude will be larger while the percentage of change will be lower. The low resistance effectively short-circuits the capacitor reducing the impedance to

$$Z = R + jw(L_1+L_2) \qquad (4\text{-}2)$$

at moderate light levels and low bias.

The effect of light intensity on the inductance, however, is unexpected since the inductance was thought to be mainly due to the bonding wire. The value of L1 and L2 are very nearly equal in all cases, showing identical variation with light intensity, and typically range between 1 nH and 2 nH. The unexpected effect is the observed increase in inductance with increasing illumination.

There was no consistent pattern to the variation of the capacitance with illumination but rather a fairly random variation. C ranges from 0.001 pF to 0.2 pF with the smaller interelectrode geometries possessing the higher capacitances.

As would be expected the smaller geometry detectors posses a lower resistance than the larger geometry detectors. In the case of the 2 x 2 μm and 2 x 3 μm detectors the 2 x 2 μm detector pos-

sesses a lower resistance at low light levels but as the light power is increased the two resistances become very nearly equal as is seen in Fig. 4.6. This follows from the same argument given for the similarity between their DC responses to light.

The effect of increasing bias is shown in Fig. 4.5 and demonstrates how the AC resistance greatly increases with bias. As the resistance increases, the effect of the capacitance becomes more and more pronounced until the net impedance becomes capacitive in nature. The complex impedance eventually simplifies to

$$Z = R/(wCR)^2 + 1/(jwC). \qquad (4\text{-}3)$$

This change from inductive to capacitive behavior would seem to suggest the possibility of a zero reactance point as observed by others [28,55]. Such a zero reactance point was not actually observed in these measurements but would appear to occur somewhere slightly under 3 volts.

The advantage of having a zero reactance bias would be an increased bandwidth by the elimination of any R/L or RC time constants if the detector was time constant limited. The impedance of the zero reactance point is determined by setting the imaginary part of Eq(1) equal to zero. If $(wCR)^2 << 1$ then Eq(1) reduces to

$$Z = (L_1 + L_2)/C \ . \qquad (4\text{-}4)$$

It should be noted that this condition is different from that of a simple resonant circuit, which is valid for only one frequency whereas Eq. (4-4) is valid as long as $(wCR)^2 << 1$ or equivalently

$\omega^2 << 1/(L_1 + L_2)C$. Using the values of inductance and capacitance at the 3 volt bias condition for the 2 x 3 m detector this would yield a resistance of approximately 240 Ohms. This is only somewhat lower than the measured average of 300 Ohms at 3 volts. It can be seen in Fig. 4.5 that the zero reactance point must occur a little before the 3 volt bias condition and therefore Eq. (4-4) seems to agree reasonably well with the measured data.

## 4.5 CURRENT DEPENDENCE ON BIAS VOLTAGE

Measurements of output AC current versus applied bias voltage reveal a nearly linear relationship between the two. Measurements were made at 500 MHz with an optical power of 800 W. Fig. 4.8 shows a typical plot of current versus bias voltage. The current increases linearly with voltage for low bias values and then slowly starts to flatten. Bias values were restricted to less than 3 volts in order to avoid electrode burn out. These plots show neither the large increase in current [55] nor the breakdown voltage [59] reported by others but agrees well with the results obtained by a GaInAs detector [30].

The predicted response from simple photoconductor theory [60] is

$$I = AqGt\mu_e V/L \qquad (4\text{-}5)$$

where A is the cross sectional area, q is the electron charge, G is the photocarrier generation rate in electron-hole pairs/cm$^3$ s, t is the average hole lifetime, $\mu_e$ is the electron mobility, V is the applied bias, and L the length between electrodes. Since all

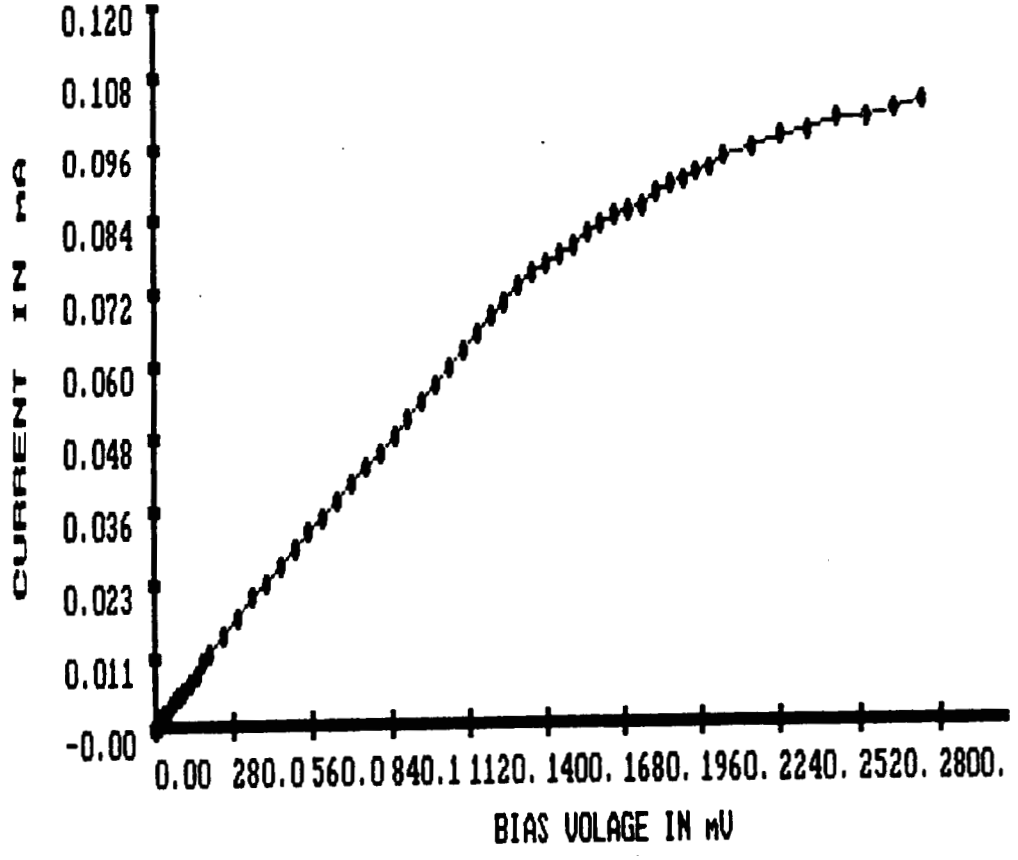


Fig. 4.8. Variation of photocurrent with bias voltage.

parameters except the applied bias were kept constant in these measurements Eq. (4-5) would predict a linear relationship between current and bias voltage. The detectors are therefore in good agreement with the theory for low bias conditions.

This simple model of Eq. (4-5) assumes that the carrier velocity is linearly proportional to the electric field

$$v_e = \mu_e E = \mu_e V/L. \qquad (4\text{-}6)$$

This is only true while the electric field E is less than the saturation electric field $E_c$ [61]. Above this critical field the carrier velocity saturates leading to the deviation in current from the predicted linear behavior. When velocity saturation is taken into account the measured data agrees very well with that predicted by theory.

## 4.6 CONCLUSIONS

Both the AC and DC impedance characteristics of the detectors have been examined. The most notable characteristics were the decrease in resistance with increasing illumination and the increase in resistance with increasing bias. A small signal model was developed and consisted of a variable resistor in parallel with a capacitor and an inductor in series with each node of the parallel RC combination. It was determined that there may indeed be a DC bias for which the detector's impedance becomes purely resistive in nature. This zero reactance point was calculated to have a value of approximately 240 Ohms and to be valid for all frequencies which satisfy the condition $(\omega CR)^2 << 1$.

The output current as a function of DC bias was also examined. The current was shown to be linearly proportional to the bias voltage for low bias values and to gradually flatten out with increasing bias. The deviation from the linear response was attributed the electron velocity saturation at fields above the critical saturation field $E_c$.

# CHAPTER 5

## CONCLUSIONS AND REMARKS

In this thesis the fabrication and properties of interdigitated photoconductors on a HEMT structure have been presented. The fabrication process used was completely compatible with that used to fabricate MODFET's making these detectors easily integrable for MMIC usage. It should be remembered that the focus of the thesis was to determine whether such detectors on an AlGaAs/GaAs heterostructure could exhibit performance at least comparable to that achieved by GaAs technology.

The detectors of various electrode geometries exhibited no difference in response to modulated light. The detectors all had a 3 dB bandwidth of 185 MHz followed by a roll-off in response of 12 dB/decade until a second plateau at 1 GHz to 2 GHz after which the response fell at the standard 20 dB/decade.

The absence of any change in bandwidth indicates that the detectors are not transit time limited. It was proposed in Chapter 3 that trapping of minority hole carriers was the determinant factor in the response of the detectors. The interelectrode geometry effect is only seen in the magnitude of the response as the gain is inversely proportional to the transit time. This effect is not always readily apparent, however, due to differing

coupling efficiencies from one detector to another.

The quantum efficiency of the various detectors was calculated from responsivity measurements and presented in Chapter 3. The quantum efficiencies presented should be taken as being lower than what would be possible to obtain from packaged detectors. This is because of difficulties in establishing a perfectly normal incident beam with the test fixtures used and variation in distance from the surface of the detectors. These factors make it impossible to determine how much of the incident light is being reflected or being absorbed outside of the active area.

The responsivity of the detectors was measured to be as high as 2.5 A/W, leading to a corresponding external quantum efficiency of 3.81. It was proposed that this quantum efficiency could be increased by as much as 30% by applying an antireflection coating to the surface of the detectors.

In Chapter 4 both the AC and DC characteristics of the detectors were examined. The detectors were shown to be symmetrical devices whose operation was independent of bias polarity. The variation in impedance with changing light intensity and DC bias were also examined and a corresponding small signal model developed. The small signal model consisted of a parallel RC combination with a series inductance attached to each node of the RC combination. The most prominent effect of changing illumination was shown to be on R which dramatically decreased with increasing illumination.

By increasing the DC bias across the detectors the impedance

was shown to change from being inductive in nature to being capacitive. The reason for this change was that at low bias the small resistance effectively short-circuited the capacitor. As the bias was increased the resistance also increased making the effect of the capacitor more and more pronounce until the net impedance was capacitive in nature. This change from inductive to capacitive reactance suggested the possibility of a zero reactance bias condition. This zero reactance point was shown to exist for all frequencies such that $(wCR)^2 << 1$.

In conclusion it should be noted that while these detectors did not exhibit an extremely high bandwidth they did posses usable gain well into the GHz range. For some applications the frequency at which a certain signal-to-noise ratio is still obtainable is of more interest than the 3 dB bandwidth. For such applications these detectors would be well suited.

## BIBLIOGRAPHY


[ 1] H. Blauvelt and H. Yen, "Transmitter and Receiver Design for Microwave Fiber Optic Links," SPIE Proc. vol. 477, pp. 44-47, 1984.

[ 2] T. R. Joseph, W. E. Stephens, and B. U. Chen, "Fiber Optic RF Links," SPIE Proc., vol. 477, pp. 52-56, 1984.

[ 3] D. S. Henry, "Lightwave Primer," IEEE J. Quantum Electron., vol. QE-21, p. 1963, 1985.

[ 4] W. D. Warters, "Milimeter Waveguide Scores High in Field Test," Bell Lab Rec., vol. 53, p. 406, 1975.

[ 5] K. B. Bhasin and D. J. Connolly, "Advances in Gallium Arsenide Monolithic Microwave Integrated-Circuit Technology for Space Communications Systems," IEEE Trans. Microwave Theory Tech., vol. MTT-34, pp. 994-1001, 1986.

[ 6] R. R. Kunath and K. B. Bhasin, "Optically Controlled Phased Array Antenna Concepts Using Monolithic Microwave Integrated Circuits," Presented at Int. IEEE Symposium, Philadephia, PA, 1986.

[ 7] L. H. Camitz, P. J. Tasker, H. Lee, D. Ban Der Merwe, and L. F. Eastman, "Microwave Characterization of Very High Transconductance MODFET," IEDM Tech. Digest, pp. 360-363, 1984.

[ 8] H. Lee, W. J. Schaff, G. W. Wicks, L. F. Eastman, and A. R. Calawa, "Optimized GaAs/(Al,Ga)As Modulation Doped Heterostructures," Presented at 11th Int. GaAs Symp. on GaAs & Related Compounds, Biarritz, September 26-28, 1984.

[ 9] Hadis Morkoc and Paul M. Solomon, "The HEMT: a Super-fast Transistor," IEEE Spectrum, pp. 28-35, February, 1984.

[11] Robert B. Darling and John P. Uyemura, "Optical Gain and Large-signal Characteristics of Illuminated GaAs MESFET's," IEEE J. Quantum Electron., vol. QE-23, pp. 1160-1171, 1987.

[12] Takayuki Sugeta and Yoshihiko Mizushima, "HighSpeed Photoresponse Mechanism of a GaAs- MESFET," Jpn. J. Appl. Phys., vol. 19, pp. L27-L29, Jan. 1980.

[13] W. D. Edwards, "Two and Three Terminal Gallium Arsenide FET Optical Detectors," IEEE Electron Device Lett., vol. EDL-1, pp. 149-150, 1980.

[14] Alvara Augusto A. DeSalles, "Optical Control of GaAs MESFET's," IEEE Trans. Microwave Theory Tech., vol. MTT-31, pp. 812-820, 1983.

[15] Elmer H. Hara and R. Ian MacDonald, "Characteristics of a Photoconductive Detector as an Optolectronic Switch," IEEE J. Quantum Electron., vol. QE-19, pp. 101-105, 1983.

[16] C. Baack, S. Elze and G. Walf, "GaAs MESFET High-Speed Optical Detector," Electronics Lett., vol. 13, p. 193, 1977.

[17] J. P. Vilcot, D. Decoster, and L. Raczy, "Noise and Dynamical Gain Studies of GaAs Photoconductive Detectors," Electronics Lett., vol. 20, pp. 274-275, 1984.

[18] C. W. Slayman and L. Figueroa, "Frequency and Pulse Response of a Novel High Speed Interdigital Suface Photoconductor (IDPC)," IEEE Electron Device Lett., vol. EDL-2, pp. 112-114, 1981.

[20] S. Y. Wang, D. M. Bloom, and D. M. Collins, "GaAs Schottky Photodiode with 3dB Bandwidth of 20 GHz," IEDM Tech. Digest, pp. 521-524, 1982.

[21] H. Blauvelt, G. Thurmond, J. Parsons, D. Lewis, and H. Yen, "Fabrication and Characterization of GaAs Schottky Barrier Photodetectors for Microwave Fiber Optic Links," Appl. Phys. Lett., vol. 45, pp. 195-196, 1984.

[22] C. J. Wei, H. J. Klein, H. Beneking, "Symmetrical Mott Barrier as a Fast Photodetector," Electronics Lett., Vol 17, pp. 688-689, 1981.

[23] S. Y. Wang and D. M. Bloom, "100 GHz Bandwidth Planar GaAs Schottky Photodiode," Electronics Lett., vol. 19, pp. 554-555, 1983.

[24] Walter Roth, Hermann Schumacher, Jurgen Kluge, H. J. Geelen, and Heinz Beneking, "The DSI Diode- A Fast Large-Area Optoelectronic Detector," IEEE Trans. Electron Devices, vol. ED-32, pp. 1034-1036, 1984.

[25] Hideki Mizuno, "Microwave Characteristics of an Optically Controlled GaAs MESFET," IEEE Trans. Microwave Theory Tech., vol. MTT-31, pp. 596-599, 1983.

[26] C. Y. Chen, B. L. Kasper, and H. M. Cox, "High-Sensitivity GaInAs Photoconductive Detectors Prepared by Vapor Phase Epitaxy," Appl. Phys. Lett., vol. 44, pp. 1142-1144, 1984.

[27] C. Y. Chen, Y. M. Pang, K. Alavi, A. Y. Cho, and P. A. Garbinski, "Interdigitated AlInAs/GaInAs Photoconductive Detectors," Appl. Phys. Lett., vol. 44, pp. 99-101, 1984.

[28] C. Y. Chen, B. L. Kasper, H. M. Cox, and J. K. Plourde, "2-Gb/s Sensitivity of a GaInAs Photoconductive Detector/GaAs Field-Effect Transitor Hybrid Photoreceiver," Appl. Phys. Lett., vol. 46, pp. 379-381, 1985.

[29] C. Y. Chen, Y. M. Pang, P. A. Garbinski, A. Y. Cho, and K. Alavi, "Modulation-doped GaInAs/AlInAs Planar Photoconductive Detectors for 1.0-1.55 uM Applications," Appl. Phys. Lett., vol. 43, pp. 308-310, 1983.

[30] John C. Gammel, Hideo Ohno, and Joseph M. Ballantyne, "High-Speed Photoconductive Detectors Using GaInAs," IEEE J. Quantum Electron., vol. QE-17, pp. 269-272, 1981.

[31] G. W. Taylor and J. G. Simmons, "High-Speed Integrated Heterojunction Field-Effect Transistor Photodetector: A Gated Photodetector," Appl. Phys. Lett., vol. 50, pp. 1754-1756, 1987.

[32] W. A. Hughes and D. G. Parker, "Operation of a High-Frequency Photodiode-Hemt Hybrid Photo-reciever at 10 GHz," Electronics Lett., vol. 22, pp. 509-510, 1986.

[33] C. Y. Chen, A. Y. Cho, C. G. Bethea, P. A. Garbinski, Y. M. Pang, and B. F. Levine, "Ultrahigh Speed Modulation-Doped Heterostructure Field-Effect Photodetectors," Appl. Phys. Lett., vol. 42, pp. 1040-1042, 1983.

[34] Tokuo Umeda, Yoshio Cho, and Akihiro Shibatomi, "Picosecond HEMT Photodetector," Japan. J. Appl. Phys., vol. 25, pp. L801-L803, 1986.

[35] K. B. Bhasin, R. N. Simons, and S. Wojtczuk "Detection of Radio-Frequency Modulated Optical Signals by Two and Three Terminal Microwave Devices," SPIE Proc. vol. 789, pp. 60-66, 1987.

[36] C. Y. Chen, Y. M. Pang, A. Y. Cho, and P. A. Garbinski, "New Minority Hole Sinked Photoconductive Detector," Appl. Phys. Lett., vol. 43, pp. 1115-1117, 1983.

[37] C. Y. Chen, A. Y. Cho, C. B. Bethea, and P. A. Garbinski, "Bias-free Selectively Doped AlGaAs-GaAs Picosecond Photodetectors," Appl. Phys. Lett., vol. 41, pp. 282-284, 1982.

[38] K. K. Choi, B. F. Levine, C. G. Bethea, J. Walker, and R. J. Malik, "Multiple Quantum Well 10 uM GaAs/AlGaAs Infared Detector with Improved Responsivity," Appl. Phys. Lett., vol. 50, pp. 1814-1816, 1987.

[39] B Jalali, H. L. Evans, and E. S. Yang, "Carrier Con-finement Photoconductive Detector," Appl. Phys. Lett., vol. 52, pp. 1323-1325, 1988.

[40] Alan W. Swanson, "The Pseudomorphic HEMT," Microwaves & RF, pp. 139-150, March, 1987.

[41] W. I. Wang, S. Judaprawira, C. E. C. Wood, and L. F. Eastman, "Molecular Beam Epitaxial GaAs-AlGaAs Heterostructures for Metal Semiconductor Field Effect Transitor Applications," Appl. Phys. Lett., vol. 38, pp. 708-710, 1981.

[42] F. Hobar Boudebous, D. Pascal, and S. Laval, "A Com-parison of Interdigital and Straight Structures for a Photoconductive Detector," IEEE Trans. Electron Devices, vol. ED-32, pp. 836-837, 1985.

[43] Ralph E. Williams, Gallium Arsenide Processing Techniques, (Artech House, 1984).

[44] R. A. Logan and F. K. Reinhart, "Optical Waveguides in GaAs-AlGaAs Epitaxial Layers," J. Appl. Phys., vol. 44, pp. 4172-4176, 1973.

[45] Nadav Bar-Chaim, Shlomo Margalit, Amnon Yariv, and Israil Ury, "GaAs Integrated Optoelectronics," IEEE Trans. Electron Devices, vol. ED-29, pp. 1372-1381, 1982.

[46] Robert B. Darling, "Analysis of Microwave Characteris-tics of Photoconductive IC Structures," J. Lightwave Tech., vol. LT-5, pp. 325-339, 1987.

[47] Robert B. Darling, "Transit-Time Photoconductivity in High-Field FET Channels," IEEE Trans. Electron Devices, vol. ED-34, pp. 433-443, 1987.

[48] Heinz Beneking, "On the Response Behavior of Fast Photoconductive Optical Planar and Coaxial Semiconductor Detectors," IEEE Trans. Electron Devices, vol. ED-29, pp. 1431-1441, 1982.

[49] Heinz Beneking, "Gain and Bandwidth of Fast Near-Infrared Photodetectors: A Comparison of Diodes, Phototransistors, and Photoconductive Devices," IEEE Trans. Electron Devices, vol. ED-29, pp. 1420-1430, 1982.

[50] George J. Papaionannou and John R. Forrest, "On the Photoresponse of GaAs MESFET's: Backgating and Deep Traps Effect," IEEE Trans. Electron Devices, vol. ED-33, pp. 373-378, 1986.

[51] G. J. Papaioannou, C. D. Kourkoutas, N. G. Theofanous, and A. T. Arapoyianni, "A Study of the Gain Mechanisms in GaAs Planar Optical Photoconductive Detectors," Physica Status Solidi, pp. K141-K146, 1987.

[52] W. T. Tsang, ed., Semiconductors and Semimetals, vol. 22; Lightwave Communications Technology, Part D, Photodetectors, (Academic Press, 1985).

[53] Dennis L. Mattock and Roger W. Forrest, "New Strides for Photodectors," Photonics Spectra, p. 141, May 1988.

[54] Junho Baek, Michael S. Shur, Kang W. Lee and Tho Vu, "Current-Voltage Characteristics of Ungated GaAs FET's," IEEE Trans. Electron Devices, vol. ED-32, No. pp. 2426-2430, 1985.

[55] Steven J. Wojtczuk, and Joseph Merrill Ballantyne, "Impedance Properties and Broad- Band Operation of GaAs Photconductive Detectors," J. Lightwave Tech., vol. Lt-5, pp. 320-324, 1987.

[56] "Touchstone", Copyright 1983, 1984, 1985, 1986, 1987, 1988, EEsof Inc. USA.

[57] Om P. Gandhi, Microwave Engineering and Applications, 1981.

[58] J. L. Gautier, D. Pasquet, and P. Pouvil, "Optical Effects on the Static and Dynamic Characteristics of a GaAs MESFET," IEEE Trans. Microwave Theory Tech., vol. MTT-33, pp. 819-822, 1985.

[59] L. Figueroa and C. W. Slayman, "A Novel Heterostructure Interdigital Photodetector (HIP) with Picosecond Optical Response," IEEE Electron Device Lett., vol. EDL-2, pp. 208-210, 1981.

[60] A. Rose, Concepts in Photoconductivity and Allied Problems, (Interscience, 1963).

[61] Guan-Wu Wang and Walter H. Ku., "An Analytical and Computer-Aided Model of the AlGaAs/GaAs High Electron Mobility Transistor," IEEE Trans. Electron Devices, vol. ED-33, pp. 657-663, 1986.

# APPENDIX A

## COMPUTER PROGRAMS

This appendix contains the listings of programs which were either used in the collection or analysis of data pertaining to detector characteristics. Each listing describes what function(s) the program performs and any other pertinent information. Anyone with a elementary understanding of BASIC and PASCAL should be able to follow the programs.

```
10    !*************************************************************************
20    !
30    !       PROGRAM NAME:       DECLOG
40    !
50    !       PURPOSE:            THIS PROGRAM COMBINES TWO FREQUENCY RESPONSE
60    !                           FILES (A LOW AND A HIGH FREQUENCY) TO PRODUCE
70    !                           A SINGLE BODE PLOT OF THE ENTIRE RANGE.  THE
80    !                           EFFECTS DUE TO THE LASER AND MEASURING SYSTEM
90    !                           CAN BE REMOVED IF SO DESIRED BY ANSWERING "Y"
100   !                           TO THE APPROPRIATE PROMPT.
110   !
120   !
130   !       WRITTEN BY:         SCOTT M. HILL
140   !
150   !       REVISION DATE:      APRIL 25, 1988
160   !
170   !       NOTES:
180   !
190   !
200   !*************************************************************************
210   !
220   !*************************************************************************
230   !       DIMENSIONING OF ARRAYS AND VARIABLE INITIALIZATION
240   !*************************************************************************
250   !
260   DIM Title$[100]
270   DIM Laser1(1001)
280   DIM Laser2(1001)
290   DIM Corr(1001)
300   DIM Amp1(1001)
310   DIM Amp2(1001)
320   CSIZE 4
330   Dbdiv=10
340 !
350 !*************************************************************************
360 !     CLEAR GRAPHICS AND TEXTS SCREENS; SET PRINTING DEVICE TO LINE PRINTER
370 !*************************************************************************
380 !
390 GCLEAR
400 OUTPUT 1;CHR$(12)
410 PRINTER IS 701
411 !
412 !*************************************************************************
413 ! IF SO DESIRED, READ IN LASER RESPONSE FILES IN ORDER REMOVE LASER EFFECTS
414 !*************************************************************************
415 !
420 INPUT "DO YOU WISH TO REMOVE THE LASER EFFECTS?",Reply$
430 IF Reply$="N" THEN GOTO 480
440 ASSIGN @Ref TO "LTSL1000"
450 ENTER @Ref;Start1,Stop1,Step1,Laser1(*)
460 ASSIGN @Ref TO "TSL1000"
470 ENTER @Ref;Start2,Stop2,Step2,Laser2(*)
471 !
472 !*************************************************************************
473 !  READ IN FREQUENCY RESPONSE FILES AND CALCULATE RESOLUTION OF DATA POINTS
474 !*************************************************************************
475 !
480 INPUT "ENTER THE NAME OF THE LOW FREQUENCY FILE:",Name1$
490 INPUT "ENTER THE NAME OF THE HIGH FREQUENCY FILE:",Name2$
500 ASSIGN @Data TO Name1$
510 ENTER @Data;Start1,Stop1,Step1,Amp1(*)
```

```
520 ASSIGN @Data TO Name2$
530 ENTER @Data;Start2,Stop2,Step2,Amp2(*)
540 Resol1=(Stop1-Start1)/1000
550 Resol2=(Stop2-Start2)/1000
551 !
552 !*************************************************************************
553 !    IF CHOSEN, REMOVE THE LASER AND SYSTEM EFFECTS
554 !*************************************************************************
555 !
560 Diff=(Amp1(987)-Laser1(987)-10)-(Amp2(9)-Laser2(9))
570 FOR X=1 TO 1001
580 Amp1(X)=Amp1(X)-Laser1(X)-10
590 Amp2(X)=Amp2(X)-Laser2(X)+Diff
600 NEXT X
601 !
602 !*************************************************************************
603 !     DRAW THE APPROPIATE GRID FOR PLOTTING THE DATA ON
604 !*************************************************************************
605 !
610 ALPHA OFF
620 GRAPHICS ON
630 GCLEAR
640 INPUT "ENTER LEFT AND RIGHT FREQUENCY TO BE PLOTTED",Left,Right
650 Left=LGT(Left)
660 Right=LGT(Right)
670 Mleft=Left-(Right-Left)*.10
680 Mright=Right+(Right-Left)*.10
690 WINDOW Mleft,Mright,-100,0
700 CLIP Left,Right,-90,0
710 CLIP ON
720 PEN 4
730 GRID MIN((Right-Left),1),Dbdiv,Left
740 CLIP OFF
750 FOR X=-90 TO 0 STEP Dbdiv
760 MOVE Mleft,X
770 LABEL USING "K";X
780 NEXT X
790 MOVE (Mright-Mleft)*.25+Mleft,-100
800 LABEL "FREQUENCY IN GHZ (LOG SCALE)"
810 FOR X=Left TO Right
820 MOVE X,-95
830 LABEL USING "K";DROUND(10^X,3)
840 NEXT X
850 MOVE Right,-95
860 LABEL USING "K";DROUND(10^Right,3)
870 CLIP ON
880 PEN 5
890 MOVE Left,Amp1(1)
891 !
892 !*************************************************************************
893 !     PLOT THE RESPONSE VERSUS THE LOG OF FREQUENCY
894 !*************************************************************************
895 !
900 FOR F=Start1 TO 2.04 STEP Step1
910 X=(F-Start1)/Resol1+1
920 DRAW LGT(F),Amp1(X)
930 NEXT F
940 FOR F=2.04 TO Stop2 STEP Step2
950 X=(F-Start2)/Resol2+1
960 DRAW LGT(F),Amp2(X)
970 NEXT F
```

```
971 !
972 !*************************************************************************
973 !    IF DESIRED, PRINT A HARD COPY OF THE DISPLAY WITH TITLE
974 !*************************************************************************
975 !
980 INPUT "DO YOU WANT A HARD COPY OF THE GRAPH?",Reply$
990 IF Reply$<>"Y" THEN GOTO 1060
1000 INPUT "ENTER THE TITLE FOR THE GRAPH:",Title$
1010 PRINT " "
1020 PRINT Title$
1030 PRINT " "
1040 DUMP GRAPHICS
1050 PRINT " "
1051 !
1052 !*************************************************************************
1053 !    IF DESIRED, VIEW A DIFFERENT PORTION OF THE RESPONSE OR ZOOM
1054 !*************************************************************************
1055 !
1060 INPUT "DO YOU WISH TO CHANGE LEFT AND RIGHT LIMITS",Reply$
1070 IF Reply$="Y" THEN GOTO 630
1080 INPUT "DO YOU WISH TO DO ANOTHER PLOT?",Reply$
1090 IF Reply$<>"Y" THEN GOTO 1120
1100 GCLEAR
1110 GOTO 480
1120 GCLEAR
1130 PRINTER IS CRT
1140 END
```

```
10  !*************************************************************************
20  !
30  !
40  !     PROGRAM NAME:      RESP
50  !
60  !
70  !     PURPOSE:           THIS PROGRAM WILL OBTAIN THE FREQUENCY RESPONSE OF A
80  !                        SYSTEM DRIVEN BY THE HP 8350B SWEEP GENERATOR AND
90  !                        TERMINATED AT THE HP 8566A SPECTRUM ANALYZER.  THE
100 !                        USER IS ASKED TO INPUT START AND STOP FREQUENCIES
110 !                        AS WELL AS POWER LEVEL FOR THE SWEEP GENERATOR.
120 !                        THE FREQUENCIES ARE SWEPT IN 20 MHZ INCREMENTS.
130 !
140 !
150 !
160 !
170 !     WRITTEN BY:        SCOTT M. HILL
180 !
190 !
200 !     REV. DATE:         MARCH 17,1988
210 !
220 !
230 !
240 !     NOTES:
250 !
260 !
270 !
280 !*************************************************************************
290 !
300 !*************************************************************************
310 !     DIMENSIONING AND VARIABLE INITIALIZATION
320 !*************************************************************************
330 !
340 Numscans=3
350 Dbdiv=10
370 DIM Title$[100]
380 DIM Amp(1001)
390 DIM Temp(1001)
400 DIM Raw(1001,5)
410 !
420 !*************************************************************************
430 !     READ IN START AND STOP FREQUENCY AND POWER LEVEL
440 !*************************************************************************
450 !
460 INPUT "ENTER THE START AND STOP FREQUENCIES IN GHZ",Sttfrq,Stpfrq
470 INPUT "ENTER THE POWER LEVEL IN dBm",Dbm
480 Resol=(Stpfrq-Sttfrq)/1000
481 Frqstep=(Stpfrq-Sttfrq)/500
490 !
500 !*************************************************************************
510 !    CLEAR GRAPHICS AND TEXT SCREENS
520 !*************************************************************************
530 !
540  OUTPUT CRT;CHR$(12)
550  GCLEAR
560  !
570  !*************************************************************************
580  !     SET UP SPECTRUM ANALYZER AND SWEEP GENERATOR
590  !*************************************************************************
600  !
601  IF Sttfrq>=2.0 THEN Setup=1
```

```
602  IF Sttfrq<2.0 THEN Setup=2
610 OUTPUT 718;"RC ";Setup
620 OUTPUT 718;"FA";Sttfrq;"GZ"
630 OUTPUT 718;"FB";Stpfrq;"GZ"
640 OUTPUT 719;"PL ";Dbm;" DM"
650 OUTPUT 719;"RF1"
660 WAIT 10
670 !
680 !*************************************************************************
690 !     STEP THROUGH FREQUENCIES AND READ IN MAGNITUDE OF RESPONSE
700 !*************************************************************************
710 !
720 FOR Scan=1 TO Numscans
730 OUTPUT 718;"A1"
740 OUTPUT 718;"A2"
750 OUTPUT 719;"CW";Sttfrq;"GZ"
760 OUTPUT 719;"SS";Frqstep;"GZ"
770 FOR F=Sttfrq TO Stpfrq STEP Frqstep
780 WAIT .35
790 OUTPUT 719;"UP"
800 NEXT F
810 OUTPUT 718;"TA"
820 FOR Point=1 TO 1001
830 ENTER 718;Raw(Point,Scan)
840 NEXT Point
850 NEXT Scan
860 !
870 !*************************************************************************
880 !     AVERAGE THE RESPONSE OVER THE NUMBER OF SCANS TAKEN
890 !*************************************************************************
900 !
910 FOR Point=1 TO 1001
920 FOR Scan=1 TO Numscans
930 IF Raw(Point,Scan)>0 THEN Raw(Point,Scan)=Raw(Point-1,Scan)
940 Temp(Point)=Temp(Point)+Raw(Point,Scan)
950 NEXT Scan
960 Amp(Point)=DROUND(Temp(Point)/Numscans,3)
970 NEXT Point
980 !
990 !*************************************************************************
1000!     GOTO THE SUBROUTINE FOR PLOTTING THE GRAPH
1010!*************************************************************************
1020!
1030 GOSUB 1570
1040!
1050!*************************************************************************
1060!     GENERATE A HARD COPY OF THE GRAPH ON THE PRINTER
1070!*************************************************************************
1080!
1090 INPUT "DO YOU WANT A HARD COPY?",Reply$
1100 IF Reply$<>"Y" THEN GOTO 1230
1110 INPUT "ENTER TITLE FOR THE GRAPH:",Title$
1120 PRINTER IS 701
1130 PRINT " "
1140 PRINT Title$
1150 PRINT " "
1160 DUMP GRAPHICS
1170 PRINT " "
1180!
1190!*************************************************************************
1200!     SAVE THE DATA ON A FLOPPY DISKETTE
```

```
1210!*******************************************************************************
1220!
1230 INPUT "DO YOU WISH TO SAVE ON DISK?",Reply$
1240 IF Reply$<>"Y" THEN GOTO 1430
1250 INPUT "ENTER FILENAME FOR DATA:",Name$
1260 ON ERROR GOTO 1290
1270 CREATE ASCII Name$,32
1280 GOTO 1360
1290 IF ERRL(1270) THEN GOTO 1330
1300 PRINT ERRM$
1310 GCLEAR
1320 PAUSE
1330 PURGE Name$
1340 WAIT 5
1350 CREATE ASCII Name$,32
1360 ASSIGN @Data TO Name$;FORMAT ON
1370 OUTPUT @Data;Sttfrq,Stpfrq,Frqstep,Amp(*)
1380 !
1390 !*******************************************************************************
1400 !     CLEAR GRAPHICS AND TEXT SCREENS AND END THE PROGRAM
1410 !*******************************************************************************
1420 !
1430 GCLEAR
1440 LOCAL 718
1450 LOCAL 719
1460 PRINTER IS CRT
1470 GOTO 1990
1480 !
1490 !*******************************************************************************
1500 !     SUBROUTINE FOR PLOTTING THE GRAPH
1510 !*******************************************************************************
1520 !
1530 !*******************************************************************************
1540 !     DRAW THE GRID FOR PLOTTING THE DATA ON
1550 !*******************************************************************************
1560 !
1570 CSIZE 4
1580 ALPHA OFF
1590 GRAPHICS ON
1600 Left=Sttfrq
1610 Right=Stpfrq
1620 Mleft=Left-(Right-Left)*.10
1630 Mright=Right+(Right-Left)*.10
1640 WINDOW Mleft,Mright,-100,0
1650 CLIP Left,Right,-90,0
1660 CLIP ON
1670 PEN 4
1680 GRID (Right-Left)/10,Dbdiv,Left
1690 CLIP OFF
1700 FOR X=-90 TO 0 STEP Dbdiv
1710 MOVE Mleft,X
1720 LABEL USING "K";X
1730 NEXT X
1740 MOVE (Mright-Mleft)*.35+Mleft,-100
1750 LABEL "FREQUENCY IN GHZ"
1760 FOR X=Left TO Right STEP (Right-Left)/10
1770 MOVE X,-95
1780 LABEL USING "K";X
1790 NEXT X
1800 MOVE Right,-95
1810 LABEL USING "K";Stpfrq
```

```
1820 !
1830 !*****************************************************************************
1840 !     PLOT THE DATA ON THE GRID
1850 !*****************************************************************************
1860 !
1870 PEN 5
1880 MOVE Left,Amp(1)
1890 FOR F=Sttfrq TO Stpfrq STEP Frqstep
1900 X=(F-Sttfrq)/Resol+1
1910 DRAW F,Amp(X)
1920 NEXT F
1930 RETURN
1940 !
1950 !*****************************************************************************
1960 !     RETURN TO THE MAIN PROGRAM
1970 !*****************************************************************************
1980 !
1990 END
2000 !
2010 !*****************************************************************************
```

```
{*************************************************
Program name:
     Responsivity

Purpose:
     This  program  is used to plot the responsivity of detectors
whose increase with optical power has been measured in dB.    The
variation  photodiode monitor voltage must be followed exactly as
this is a very application specific program  and  not  a  general
plotting routine.

Written by:
     Scott M. Hill

*************************************************}

PROGRAM RESPONSIVITY;
USES
  CRT,GRAPH;
LABEL
  LIMITS;

{*************************************************
 declare variables and their types
*************************************************}

TYPE
  MINE= ARRAY[0..1500]OF REAL;
  NAME_STRING=STRING[20];
  SHORT_STRING=STRING[5];
VAR
  GM,GD,ERRORCODE,X,Y,Z,COUNT,XDIV,YDIV:    INTEGER;
  LEFT,RIGHT,TOP,BOTTOM,BOTMAR,LEFTMAR,Place: INTEGER;
  XSCALE,YSCALE,MW,MA,DROP,MAXAMP,MAXPOWER: REAL;
  RESP,WATTS: MINE;
  DATA,WATT: TEXT ;
  MILAMP,REPLY:  SHORT_STRING;
  NAME: NAME_STRING;

{*************************************************
 function used to raise a number to its specified
 exponent  (used for calculating 10^x
*************************************************}

FUNCTION RAISE(VALUE,POWER: REAL):REAL;
  BEGIN
    RAISE:=EXP(POWER*LN(VALUE));
  END;

{*************************************************
 enter file which contains the measured data points.
 Also enter the drop in dB between the initial
 plateau and the value at 500 MHz
*************************************************}
```

```
BEGIN
  RESTORECRTMODE;
  ClrScr;
  WRITE('INPUT NAME OF DATA FILE  ');
  READLN(NAME);
  WRITELN;
  WRITE('INPUT GAIN DROP BETWEEN 0 AND 500 MHZ  ');
  READ(DROP);
  READLN;

{*****************************************************
 enter the plotting limits for the photocurrent and
 the optical power
*****************************************************

LIMITS: CLRSCR;
  WRITE(' INPUT MAXIMUM CURRENT TO BE PLOTTED IN
          MILLIAMPS ');
  READ(MAXAMP);
  WRITELN;
  WRITE(' INPUT MAXIMUM LIGHT POWER TO BE PLOTTED IN
          MILLIWATTS ');
  READ(MAXPOWER);
  READLN;

{*****************************************************
 open the files containing the data and the
 calibration file of optical power vs monitor voltage
*****************************************************}

  WRITELN;
  ASSIGN(DATA,NAME);
  ASSIGN(WATT,'A:WATT.DAT');
  Z:=0;
  RESET(DATA);
  RESET(WATT);

{*****************************************************
 draw graph and label axis accordingly
 *****************************************************

  GD:=Detect;
  InitGraph(GD,GM,'');
  ERRORCODE:=GRAPHRESULT;
  IF (ERRORCODE <> grOK) THEN
    HALT(1);
  LEFT:=ROUND(GETMAXX*0.25);
  TOP:=0;
  RIGHT:=ROUND(GETMAXX-40);
  BOTTOM:=ROUND(GETMAXY*0.85);
  BOTMAR:=BOTTOM+8;
  LEFTMAR:=LEFT-50;
  XSCALE:=(RIGHT-LEFT)/MAXPOWER;
```

```
  YSCALE:=(TOP-BOTTOM)/MAXAMP;
  YDIV:=ROUND((BOTTOM-TOP)/10);
  XDIV:=ROUND((RIGHT-LEFT)/10);
  SETVIEWPORT(0,0,GETMAXX,GETMAXY,CLIPON);
  SETLINESTYLE(0,0,3);
  CLEARDEVICE;
  LINE(LEFT,TOP,LEFT,BOTTOM);
  LINE(LEFT,BOTTOM,GETMAXX,BOTTOM);
  COUNT:=0;
  PLACE:=TOP;

  WHILE COUNT <11 DO
    BEGIN
    STR((BOTTOM-PLACE)/-YSCALE:2:3,MILAMP);
    OUTTEXTXY(LEFTMAR,PLACE,MILAMP);
    LINE(LEFT-3,PLACE,LEFT+3,PLACE);
    PLACE:=PLACE+YDIV;
    COUNT:=COUNT+1;
    END;
  COUNT:=0;
  PLACE:=LEFT;
  WHILE COUNT <11 DO
    BEGIN
    STR((PLACE-LEFT)/XSCALE:2:2,MILAMP);
    OUTTEXTXY(PLACE,BOTMAR,MILAMP);
    LINE(PLACE,BOTTOM-3,PLACE,BOTTOM+3);
    PLACE:=PLACE+XDIV;
    COUNT:=COUNT+1;
    END;
  OUTTEXTXY(350,GETMAXY-8,'OPTICAL POWER IN mW');
  SETTEXTSTYLE(0,1,1);
  OUTTEXTXY(LEFTMAR-20,35,'CURRENT IN mA');
  OUTTEXTXY(LEFTMAR-80,0,CONCAT('RESPONSIVITY ',NAME));
  SETTEXTSTYLE(0,0,1);
  MOVETO(LEFT,BOTTOM);
  COUNT:=0;

{*****************************************************
 plot the photocurrent vs optical power
*****************************************************}

  WHILE COUNT <= 100 DO
    BEGIN
    READ(DATA,RESP[COUNT]);
    READ(WATT,WATTS[COUNT]);
    X:=ROUND((WATTS[COUNT]-0.33)*XSCALE+LEFT);
    MW:=RAISE(10,(RESP[COUNT]-35+DROP)/10);
    MA:=2*1000.0*SQRT(MW*56.0/1000)/56.0;
    Y:=ROUND(BOTTOM+MA*YSCALE);
    LINETO(X,Y);
    CIRCLE(X,Y,2);
    COUNT:=COUNT+10;
    END;
  COUNT:=125;
```

```
  WHILE COUNT <= 200 DO
    BEGIN
    READ(DATA,RESP[COUNT]);
    READ(WATT,WATTS[COUNT]);
    X:=ROUND((WATTS[COUNT]-0.33)*XSCALE+LEFT);
    MW:=RAISE(10,(RESP[COUNT]-35+DROP)/10);
    MA:=2*1000.0*SQRT(MW*56.0/1000)/56.0;
    Y:=ROUND(BOTTOM+MA*YSCALE);
    LINETO(X,Y);
    CIRCLE(X,Y,2);
    COUNT:=COUNT+25;
    END;
  COUNT:=250;
  WHILE COUNT <= 1500 DO
    BEGIN
    READ(DATA,RESP[COUNT]);
    READ(WATT,WATTS[COUNT]);
    X:=ROUND((WATTS[COUNT]-0.33)*XSCALE+LEFT);
    MW:=RAISE(10,(RESP[COUNT]-35+DROP)/10);
    MA:=2*1000.0*SQRT(MW*56.0/1000)/56.0;
    Y:=ROUND(BOTTOM+MA*YSCALE);
    LINETO(X,Y);
    CIRCLE(X,Y,2);
    COUNT:=COUNT+50;
    END;
  Z:=Z+1;
  READLN;
  CLOSEGRAPH;
  RESTORECRTMODE;
  CLRSCR;
  WRITE('DO YOU WISH TO CHANGE LIMITS OF PLOTTING  ');
  READLN(REPLY);
  IF (REPLY='Y') THEN GOTO LIMITS;
END.
```

NASA
National Aeronautics and Space Administration

# Report Documentation Page

| 1. Report No. | 2. Government Accession No. | 3. Recipient's Catalog No. |
|---|---|---|
| NASA CR-182197 | | |

**4. Title and Subtitle**
Microwave Characteristics of Interdigitated Photoconductors on a HEMT Structure

**5. Report Date**
November 1988

**6. Performing Organization Code**

**7. Author(s)**
Scott M. Hill and Paul C. Claspy

**8. Performing Organization Report No.**
None

**10. Work Unit No.**
506-44-21

**9. Performing Organization Name and Address**
Dept. of Electrical Engineering and Applied Physics
Case Western Reserve University
Cleveland, Ohio 44106

**11. Contract or Grant No.**
NCC3-99

**13. Type of Report and Period Covered**
Contractor Report
Final

**12. Sponsoring Agency Name and Address**
National Aeronautics and Space Administration
Lewis Research Center
Cleveland, Ohio 44135-3191

**14. Sponsoring Agency Code**

**15. Supplementary Notes**
Project Manager, Kul B. Bhasin, Space Electronics Division, NASA Lewis Research Center. This report was submitted by Scott M. Hill in partial fulfilment of the requirements for the degree Master of Science to Case Western Reserve University in August 1988.

**16. Abstract**

Interdigitated photoconductive detectors of various geometries have been fabricated on AlGaAs/GaAs heterostructure material. This report describes the processes used in fabrication of these devices and presents the results of a study of their optical and electrical characteristics. The fabrication process used was completely compatible with that used to fabricate MODFET's, making these detectors easily integrable for MMIC use. Detector responsivity as high as 2.5 A/W, leading to an external quantum efficiency of 3.81, was measured. It was found that response speed was independent of electrode geometry and dimensions and that all detectors had usable response at frequencies to 6 GHz, with a 3 dB frequency of 185 MHz. Because of the form of the frequency response and its independence of device geometry it is proposed that minority carrier trapping effects dominate high frequency performance. The results of DC and AC impedance measurements, as well as a small signal model of the detectors, based on those measurements is presented.

| 17. Key Words (Suggested by Author(s)) | 18. Distribution Statement |
|---|---|
| Gallium arsenide; Optical detector; HEMT photodetector; Microwave response; GaAlAs photodetector | Unclassified – Unlimited<br>Subject Category 33 |

| 19. Security Classif. (of this report) | 20. Security Classif. (of this page) | 21. No of pages | 22. Price* |
|---|---|---|---|
| Unclassified | Unclassified | 90 | A05 |



*For sale by the National Technical Information Service, Springfield, Virginia 22161